High-Spatial-Resolution Surface and Cloud-Type Classification from MODIS Multispectral Band Measurements

JUN LI

Cooperative Institute for Meteorological Satellite Studies, University of Wisconsin—Madison, Madison, Wisconsin

W. PAUL MENZEL

Office of Research and Applications, NOAA/NESDIS, Madison, Wisconsin

ZHONGDONG YANG,* RICHARD A. FREY, AND STEVEN A. ACKERMAN

Cooperative Institute for Meteorological Satellite Studies, University of Wisconsin—Madison, Madison, Wisconsin

(Manuscript received 21 December 2001, in final form 12 August 2002)

ABSTRACT

A method for automated classification of surface and cloud types using Moderate Resolution Imaging Spectroradiometer (MODIS) radiance measurements has been developed. The MODIS cloud mask is used to define the training sets. Surface and cloud-type classification is based on the maximum likelihood (ML) classification method. Initial classification results define training sets for subsequent iterations. Iterations end when the number of pixels switching classes becomes smaller than a predetermined number or when other criteria are met. The mean vector in the spectral and spatial domain within a class is used for class identification, and a final 1-km-resolution classification mask is generated for such a field of view in a MODIS granule. This automated classification refines the output of the cloud mask algorithm and enables further applications such as clear atmospheric profile or cloud parameter retrievals from MODIS and Atmospheric Infrared Sounder (AIRS) radiance measurements. The advantages of this method are that the automated surface and cloud-type classifications are independent of radiance or brightness temperature threshold criteria, and that the interpretation of each class is based on the radiative spectral characteristics of different classes. This paper describes the ML classification algorithm and presents daytime MODIS classification results. The classification results are compared with the MODIS cloud mask, visible images, infrared window images, and other observations for an initial validation.

1. Introduction

The Moderate Resolution Imaging Spectroradiometer (MODIS) is a key instrument on the Earth Observing System (EOS) for conducting global change research. It provides global observations of the earth's land, oceans, and atmosphere in 36 visible (VIS), near-infrared (NIR), and infrared (IR) regions of the spectrum from 0.4 to 14.5 μm. MODIS measurements record biological and geophysical processes on a global scale every 1–2 days in unprecedented detail.

MODIS cloud classification has many applications. MODIS atmospheric and surface parameter retrievals require cloud-free measurements (Li et al. 2001a), while cloud-type information such as single- and/or multilayer or high/medium/low cloud information will greatly benefit cloud parameter retrievals (Frey et al. 1999; Li et al. 2001b) and the derivation of cloud motion vectors (Velden et al. 1997). Cloud classification can also improve the monitoring of deep convective clouds and rainfall estimation from IR cloud imagery data (Li et al. 1992, 1993). MODIS cloud information can further the International Satellite Cloud Climatology Program (ISCCP) that was stimulated by research on several methods of cloud classification that have been tested in a systematic algorithm intercomparison (Rossow et al. 1985). In addition, clear-, single-, and/or multilayer cloud information from MODIS measurements within a single Atmospheric Infrared Sounder (AIRS) footprint (15 km) will greatly enhance the cloud clearing of partly cloudy AIRS radiances (Susskind et al. 1998) and therefore improve atmospheric temperature and moisture profiles through the synergism of MODIS and AIRS radiance measurements from the *Aqua* satellite launched

* Visiting scientist, National Satellite Meteorological Center, Beijing, China.

Corresponding author address: Dr. Jun Li, Cooperative Institute for Meteorological Satellite Studies, University of Wisconsin—Madison, 1225 West Dayton Street, Madison, WI 53706.
E-mail: junl@ssec.wisc.edu

TABLE 1. MODIS spectral band specifications.

Primary use	Band	Bandwidth[a]	Spectral radiance[b]	Required SNR[c]
Land/cloud/aerosols boundary	1	620–670	21.8	128
	2	841–876	24.7	201
Land/cloud/aerosols properties	3	459–479	35.3	243
	4	545–565	29.0	228
	5	1230–1250	5.4	74
	6	1628–1652	7.3	275
	7	2105–2155	1.0	110
Ocean color/phytoplankton/biogeochemistry	8	405–420	44.9	880
	9	438–448	41.9	838
	10	483–493	32.1	802
	11	526–536	27.9	754
	12	546–556	21.0	750
	13	662–672	9.5	910
	14	673–683	8.7	1087
	15	743–753	10.2	586
	16	862–877	6.2	516
Atmospheric water vapor	17	890–920	10.0	167
	18	931–941	3.6	57
	19	915–965	15.0	250
Primary use	Band	Bandwidth	Spectral radiance	Required NEΔT[d] (K)
Surface temperature	20	3.660–3.840	0.45 (300 K)	0.05
	21	3.929–3.989	2.38 (335 K)	2.00
	22	3.929–3.989	0.67 (300 K)	0.07
	23	4.020–4.080	0.79 (300 K)	0.07
Temperature profile	24	4.433–4.498	0.17 (250 K)	0.25
	25	4.482–4.549	0.59 (275 K)	0.25
Cirrus clouds/water vapor	26	1.360–1.390	6.00	150 (SNR)
Water vapor	27	6.535–6.895	1.16 (240 K)	0.25
	28	7.175–7.475	2.18 (250 K)	0.25
	29	8.400–8.700	9.58 (300 K)	0.05
Ozone	30	9.580–9.880	3.69 (250 K)	0.25
Surface temperature	31	10.780–11.280	9.55 (300 K)	0.05
	32	11.770–12.270	8.94 (300 K)	0.05
Temperature profile	33	13.185–13.485	4.52 (260 K)	0.25
	34	13.485–13.785	3.76 (250 K)	0.25
	35	13.785–14.085	3.11 (240 K)	0.25
	36	14.085–14.385	2.08 (220 K)	0.35

[a] Bands 1 to 19: nm; bands 20 to 36: μm.
[b] Spectral radiance values: W m^{-2} sr^{-1} μm^{-1}.
[c] SNR is signal-to-noise ratio.
[d] NEΔT is noise-equivalent temperature difference.

TABLE 2. Initial classes from MODIS cloud mask algorithm.

Class index	Content
1	Confident clear water
2	Confident clear coastal
3	Confident clear desert or semiarid ecosystems
4	Confident clear land
5	Confident clear snow or ice
6	Shadow of cloud or other clear
7	Other confident clear
8	Cirrus detected by solar bands
9	Cirrus detected by infrared bands
10	High clouds detected by CO_2 bands
11	High clouds detected by 6.7-μm band
12	High clouds detected by 1.38-μm band
13	High clouds detected by 3.7- and 12-μm bands
14	Other clouds or possible clouds
15	Undecided

on 4 May 2002. Surface and cloud-type classification and identification are very important for surface, atmospheric, and cloud property retrievals.

Researchers at the Cooperative Institute for Meteorological Satellite Studies (CIMSS) of the University of Wisconsin—Madison have developed an algorithm for clear-sky detection from MODIS measurements (Ackerman et al. 1998). The MODIS cloud mask relies on a variety of threshold tests for clear-sky and cloudy determinations. This reliance on thresholds results in limitations in special situations, such as separating low clouds in the presence of snow. To reduce the dependence on thresholds in the cloud mask algorithm, the maximum likelihood (ML) classification procedure can be used as a supplement to improve the detection of clear and cloudy skies in the MODIS imagery.

A number of researchers have addressed cloud classification from a variety of perspectives. Imagery clas-

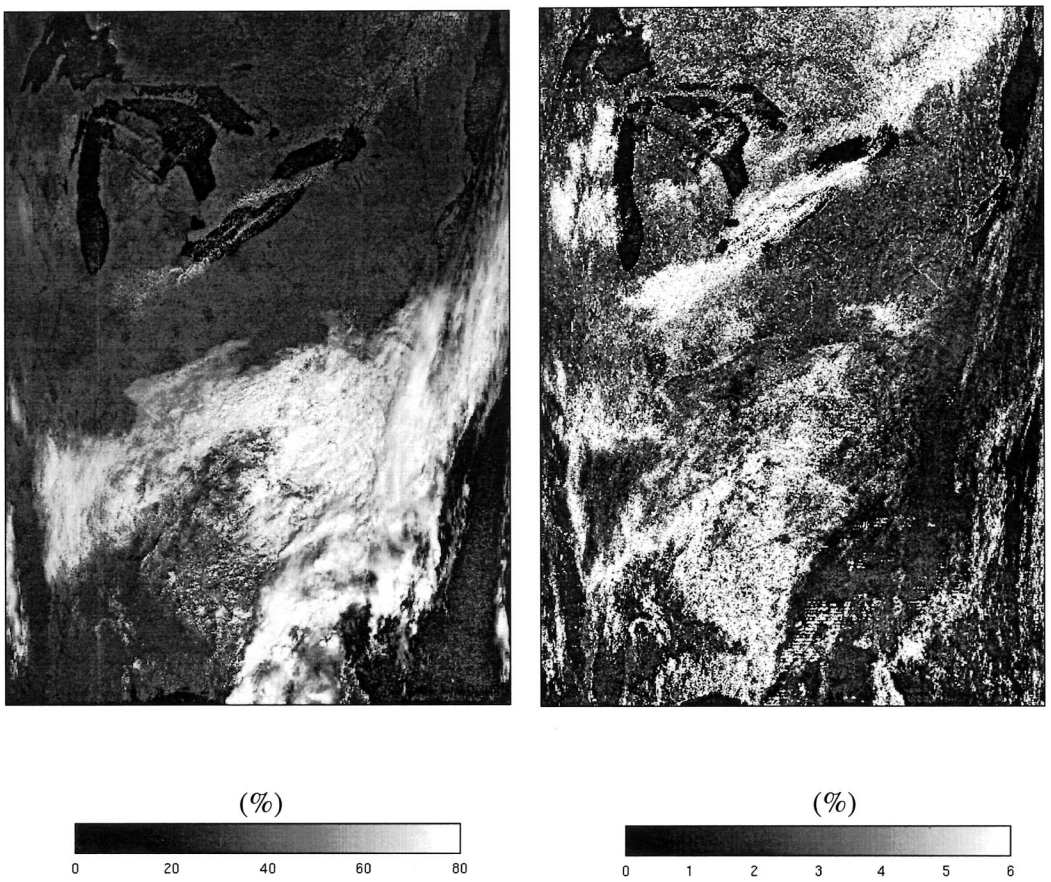

FIG. 1. (left) MODIS 0.86-μm (band 2; in units of reflectance (percent); (right) its LSD images of MODIS in percent variance. Showing are the clouds over the eastern part of the United States at 1635 UTC 5 Sep 2000.

sification studies include, but are not limited to, discrimination of cloud types in polar regions (Ebert 1987, 1989; Key et al. 1989; Key 1990; Welch et al. 1992) and in tropical scenes (Desbois et al. 1982; Inoue 1987), discrimination of ice and water clouds (Knottenberg and Raschke 1982), separation of clouds and snow (Tsonis 1984; Allen et al. 1990; Li and Zhou 1990), detection of fire and smoke (Baum and Trepte 1999), classification of ocean clouds (Garand 1988; Tag et al. 2000; Lubin and Morrow 1998), and clear-sky classification (Saunders and Kriebel 1998; Vemury et al. 2001). The classification methods include a variety of approaches such as neural networks, maximum likelihood, and fuzzy logic. In general, classification procedures can be divided into two types: supervised and unsupervised. The premise of supervised classification is the ''training'' of a classifier based on known cases of specific scenes such that the classifier, once trained, can be used with confidence on unknown cloud image samples. This method, although straightforward, entails considerable effort in the manual typing of the training samples (Tag et al. 2000). An unsupervised classification method allows the classifier to determine its own division of cloud types using a mathematical separability of classes based on designated scene or cloud radiative spectral characteristics. However, good initial classification is very important for unsupervised classification due to insufficient training data.

In this paper, the MODIS cloud mask (Ackerman et al. 1998) information is used as the initial classification for the unsupervised MODIS surface and cloud-type classification approach. The objectives of this study are to

1) provide an additional clear/cloud mask that can be used for validation or comparison with other cloud products from MODIS measurements;
2) determine a reliable clear/cloudy index for atmospheric total precipitable water (TPW) and total column ozone retrieval from MODIS clear-sky radiance measurements;
3) estimate cloud types that can greatly benefit cloud-top pressure and effective cloud amount retrievals with combined MODIS and AIRS measurements; and
4) generate clear-, single-, and/or multilayer cloud in-

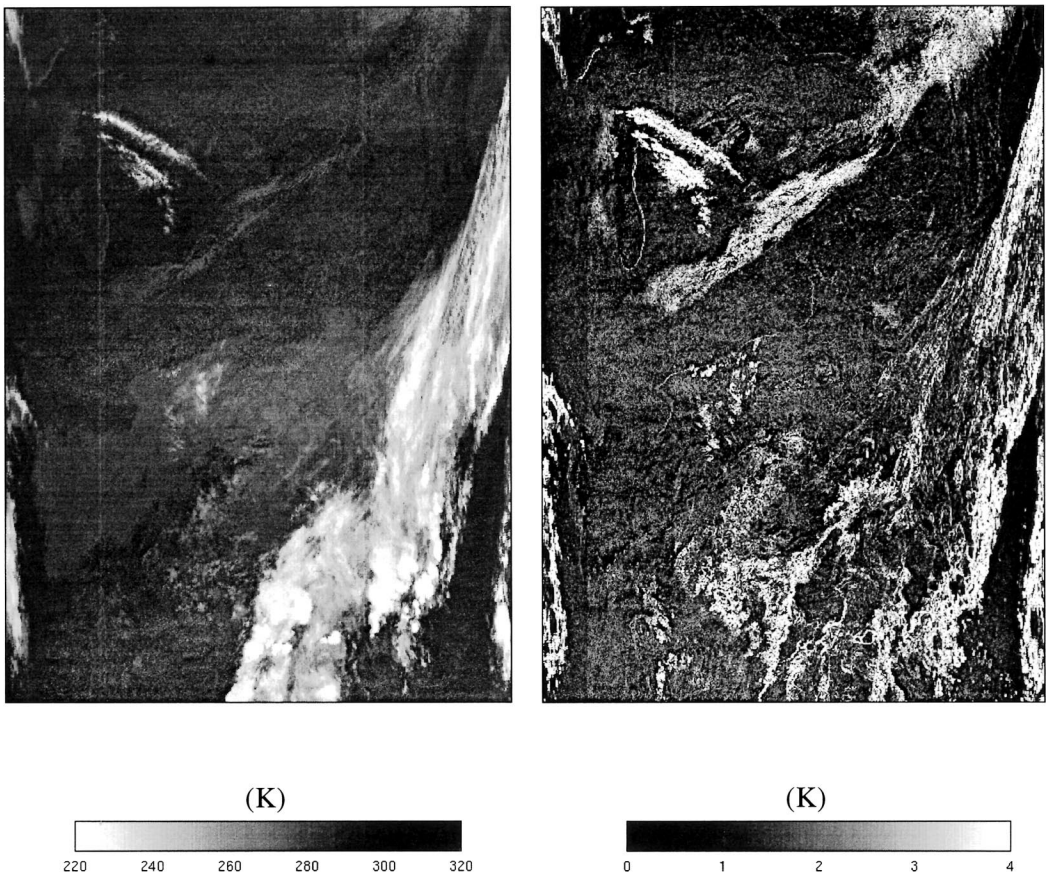

FIG. 2. (left) MODIS 11-μm (band 31) brightness temperature image (K) and (right) its LSD image. Area is the eastern part of the United States at 1635 UTC 5 Sep 2000.

formation within an AIRS footprint for better AIRS cloud clearing.

The unique features of this cloud classification study are as follows.

1) The MODIS cloud mask is used to provide a very good initial classification for the ML classifier.
2) Unlike the MODIS cloud mask that returns a confidence level of clear ranging from 1 (high) to 0 (low), the ML classifier provides a binary yes/no answer for each pixel on clear/cloud discrimination.
3) Unlike other cloud classification procedures that rely on spectral coherence in a spatial area of N by N pixels [for example, Tag et al. (2000) use 16 km by 16 km areas for advanced very high resolution radiometer (AVHRR) cloud classification], this approach uses 1-km single-field-of-view features in the classification; therefore, it returns a 1-km high-spatial-resolution classification mask.
4) The algorithms for surface and cloud-type identification in the MODIS cloud mask are also used in the ML classifier, thus reducing the error due to manual identification of each class.

Section 2 provides a description of the MODIS cloud mask algorithm. Section 3 outlines the algorithms for the scene and cloud classification with MODIS spectral band radiance measurements. Section 4 presents a summary of MODIS spectral characteristics and feature selection. Section 5 summarizes the physical basis for the identification of surface and cloud types in the ML classification mask. Section 6 describes the daytime classification and initial validation using MODIS measurements. A discussion of issues affecting classification results is given in section 7. Section 8 describes the conclusions and future work.

2. Summary of the MODIS cloud mask algorithm

MODIS measures radiances in bands 1 and 2 at 0.25-km spatial resolution, in bands 3–7 at 0.5-km resolution, and the remaining 29 bands at 1-km resolution (see Table 1 for the MODIS spectral band specification; the numbers in this table are available online at http://modis.gsfc.nasa.gov/about/specs.html). Radiances from 14 spectral bands (bands 1 and 2, bands 5 and 6, bands 18–21, bands 26 and 27, band 29, bands 31 and 32,

TABLE 3. Features used in ML classification algorithm.

Features	Unit	Used in cloud mask	Primary use
BAND 1	%	Y	Clouds, shadow
BAND 2	%	Y	Low clouds
BAND 3	%	N	
BAND 4	%	N	Snow
BAND 5	%	Y	Snow
BAND 6	%	Y	Snow, shadow
BAND 7	%	N	
LSD–BAND 1	%	N	Cirrus, low clouds, surface
LSD–BAND 2	%	N	Cirrus, low clouds, surface
LSD–BAND 3	%	N	
LSD–BAND 4	%	N	
LSD–BAND 5	%	N	Clouds, snow, surface
LSD–BAND 6	%	N	Clouds, snow, surface
LSD–BAND 7	%	N	
BAND 17	%	N	
BAND 18	%	Y	Low clouds
BAND 19	%	Y	Shadow
BAND 20	K	Y	Shadow
BAND 21	K	Y	
BAND 22	K	N	
BAND 23	K	N	
BAND 24	K	N	
BAND 25	K	N	
BAND 26	%	Y	
BAND 27	K	Y	
LSD–BAND 27	K	N	
BAND 28	K	N	
LSD–BAND 28	K	N	
BAND 29	K	Y	
BAND 31	K	Y	Clouds, surface
LSD–BAND 31	K	N	
BAND 32	K	Y	Clouds, surface
BAND 33	K	N	
BAND 34	K	N	
BAND 35	K	Y	High clouds
BT_{11}–BT_{12}	K	N	
$BT_{8.6}$–BT_{11}	K	N	Clouds
BT_{11}–$BT_{6.7}$	K	N	Clouds
$BT_{3.9}$–$BT_{3.7}$	K	N	
BT_{11}–$BT_{3.7}$	K	N	Clouds
BT_{12}–BT_{4}	K	N	
$BT_{13.7}$–BT_{14}	K	N	
BT_{11}–$BT_{3.9}$	K	N	

band 35) are used in the MODIS cloud mask algorithm (initial classification) to estimate whether a given view of the earth's surface is obstructed by clouds or optically thick aerosol, and whether a clear scene is affected by cloud shadows (Ackerman et al. 1998). The physical basis for the MODIS cloud detection is that clouds are generally characterized by higher reflectance and lower brightness temperatures than the underlying earth's surface. The MODIS cloud mask algorithm determines if a given pixel is clear by combining the results of several spectral threshold tests. A confidence level of clear sky for each ground instantaneous field of view (GIFOV) is estimated based on a comparison between observed radiances and specified thresholds. The cloud mask algorithm also uses background data such as a water–land index.

The MODIS cloud mask (information available online at http://modis-atmos.gsfc.nasa.gov/MOD35_L2/index.html) provides 15 classes. Those classes are the primary input for the initial classification of the iterative ML classification procedure. The 15 classes are listed in Table 2. The initial surface and cloud types used for the ML classification procedure varies with the number of classes one attempts to extract from the MODIS cloud mask (e.g., the 2 clear-vs-cloudy classes would be very different from the 15 classes extracted here).

3. ML classification algorithm based on the MODIS cloud mask

Classification or clustering of the radiances and local spatial distribution of the radiances is an important part of data analysis and image segmentation. A group or cluster refers to a class of data that has a similar appearance (i.e., for MODIS images, it can be a particular surface type or cloud cover). Basic data clustering does not need any external information for its completion.

In general, the distribution of each class presented in the MODIS image data can be approximated by a multivariate normal distribution, or locally normal distribution (Lee et al. 1999), and the classification procedure can be performed by the well-known ML or quadratic classifier (Haertel and Landgrebe 1999)

$$G_i(\mathbf{X}) = -(\mathbf{X} - \boldsymbol{\mu}_i)^{\mathrm{T}}\boldsymbol{\Sigma}_i^{-1}(\mathbf{X} - \mu_i) - \ln|\boldsymbol{\Sigma}_i| + 2\ln P(\omega_i), \quad (1)$$

with ω_i being a particular class, $\mathbf{X}$ an unlabeled vector of a pixel spanning the space of the radiance and spatial distribution of the radiance, $\boldsymbol{\mu}_i$ the class mean vector in that space, $\boldsymbol{\Sigma}_i$ the class covariance matrix, $P(\omega_i)$ the corresponding a priori probability for class ω_i, and $G_i(\mathbf{X})$ the discriminate function associated with class ω_i; subscript i is the index for the ith class. For simplicity, assuming that the probability $P(\omega_i)$ for each class ω_i is equal, a distance is defined to assign each pixel to particular class ω_i:

$$D_i(\mathbf{X}) = (\mathbf{X} - \boldsymbol{\mu}_i)^{\mathrm{T}}\boldsymbol{\Sigma}_i^{-1}(\mathbf{X} - \boldsymbol{\mu}_i) + \ln|\boldsymbol{\Sigma}_i|. \quad (2)$$

Mathematically, the pixel $\mathbf{X}$ is assigned to class ω_i if

$$D_i(\mathbf{X}) \le D_j(\mathbf{X}) \quad \text{for all } \omega_j \ne \omega_i. \quad (3)$$

The clustering algorithm can be described by the following steps:

1) Classify the MODIS measurements using the MODIS cloud mask, and calculate the mean vector and covariance matrix of each class within the MODIS cloud mask.
2) Calculate the distances between the vector of each pixel and mean vectors of different classes, and assign the pixel to the nearest class.

TABLE 4. Class center values of 13 classes at 1635 UTC 5 Sep 2000 (case1). The units are kelvins for IR bands and reflectance (percent) for VIS/NIR bands. See text for feature definitions.

Features	Water	Land	Land	Land	M.L. Cld	Mixed	M.L. Cld	M.L. Cld	M.H. Cld	Undecided	M.H. Cld	L. Cld	H. Cld
Percentage	9.99	15.23	7.67	18.00	4.00	3.37	4.79	8.16	6.90	0.20	5.30	13.37	2.96
Class index	1	2	3	4	5	6	8	9	10	11	12	13	15
BAND 1	3.08	4.25	9.85	5.16	22.51	8.23	29.80	17.60	60.32	30.37	55.55	58.43	72.77
BAND 2	1.74	21.43	26.68	26.75	26.27	9.40	40.10	31.13	63.15	32.38	59.14	63.91	73.44
BAND 3	9.91	8.74	15.72	8.76	28.03	14.90	33.73	21.89	64.54	36.51	59.68	61.49	76.32
BAND 4	5.29	6.53	12.37	7.35	23.95	10.12	31.45	19.31	60.40	31.83	55.87	58.68	72.22
BAND 5	1.35	21.11	28.93	27.00	24.40	8.82	37.88	30.87	48.54	27.41	48.98	53.99	53.50
BAND 6	0.92	11.68	19.69	16.55	16.07	6.66	31.23	23.53	19.60	15.18	31.06	48.63	20.98
BAND 7	0.56	4.40	8.76	6.87	9.64	4.13	20.11	14.45	9.82	8.51	17.89	30.36	11.16
LSD–BAND 1	0.28	0.59	1.40	0.86	2.40	1.98	11.70	5.91	0.87	2.88	1.61	3.25	1.19
LSD–BAND 2	0.40	3.16	2.03	2.90	2.61	2.53	11.33	6.19	0.97	3.26	1.80	3.68	2.19
LSD–BAND 3	0.16	0.25	0.64	0.30	1.81	1.27	8.63	3.61	0.75	2.19	1.23	2.09	1.05
LSD–BAND 4	0.18	0.37	0.74	0.45	1.91	1.39	9.42	3.97	0.76	2.30	1.28	2.28	1.03
LSD–BAND 5	0.27	1.87	1.58	1.30	1.89	1.77	8.28	4.04	0.96	2.34	1.71	3.60	1.78
LSD–BAND 6	0.24	1.18	1.94	1.08	1.34	1.58	8.03	4.29	0.50	1.46	1.09	1.93	0.52
LSD–BAND 7	0.21	0.65	1.44	0.84	0.95	1.21	6.26	3.73	0.37	0.96	0.87	1.47	0.36
BAND 17	1.16	18.39	18.69	23.12	22.28	6.85	31.90	24.35	51.70	25.53	46.57	47.26	55.36
BAND 18	0.65	8.77	4.51	11.15	14.59	3.20	14.57	10.00	39.92	22.76	29.51	18.00	60.16
BAND 19	0.80	12.29	8.88	15.54	17.22	4.36	20.58	14.88	45.27	24.09	36.29	27.98	61.08
BAND 20	292.53	290.62	306.35	296.64	285.05	296.69	305.49	303.34	264.35	281.89	284.76	307.03	262.01
BAND 21	291.46	288.49	304.43	294.16	277.43	293.82	296.32	296.04	250.19	273.40	272.31	295.60	241.86
BAND 22	291.67	288.67	304.94	294.53	277.77	294.23	296.96	296.61	250.20	272.92	272.44	296.35	241.11
BAND 23	288.69	285.45	300.60	290.47	273.32	290.18	290.96	291.23	246.92	268.46	267.30	289.44	236.43
BAND 24	250.30	248.45	254.43	253.36	240.85	249.76	252.12	251.52	232.05	238.31	239.69	251.82	225.01
BAND 25	268.99	266.13	275.70	271.40	252.88	268.05	268.21	268.80	234.37	247.83	247.18	266.57	221.48
BAND 26	0.21	0.62	0.60	0.73	6.52	1.07	1.71	1.13	15.38	11.91	7.93	1.92	31.88
BAND 27	244.66	245.72	246.48	250.15	233.63	239.79	247.14	246.29	230.05	233.47	233.88	245.47	223.87
LSD–BAND 27	0.64	0.61	0.68	0.53	1.42	0.98	0.58	0.61	0.97	10.01	0.83	0.61	1.27
BAND 28	260.11	260.57	260.85	265.14	244.21	254.42	261.11	260.79	234.93	241.48	243.05	260.27	225.14
LSD–BAND 28	0.43	0.41	0.57	0.35	2.47	1.27	0.52	0.50	1.25	12.94	1.17	0.48	1.36
BAND 29	286.79	284.97	294.43	289.04	261.52	283.71	282.24	284.31	239.67	258.13	253.05	278.45	226.89
BAND 31	289.98	286.93	296.85	291.65	259.85	285.05	284.08	286.21	237.94	257.39	252.10	280.81	224.62
LSD–BAND 31	0.40	0.74	0.98	0.78	5.12	3.01	2.48	1.97	1.81	24.21	2.17	0.90	1.57
BAND 32	288.47	286.59	294.74	291.41	257.77	283.12	283.01	284.98	237.32	256.19	251.01	280.33	224.28
BAND 33	266.05	265.00	268.91	270.13	245.71	261.88	265.83	265.74	233.77	243.66	243.97	264.96	223.19
BAND 34	253.63	252.75	256.26	256.62	239.17	250.94	255.47	254.79	231.01	237.46	239.16	255.20	222.17
BAND 35	245.68	245.14	247.98	248.17	234.84	243.70	247.74	247.05	228.76	233.37	235.16	247.50	221.60
BT_{11}–BT_{12}	1.09	0.33	2.01	0.27	2.08	1.87	1.10	1.17	0.65	1.20	1.10	0.48	0.39
$BT_{8.6}$–BT_{11}	−2.60	−2.30	−2.36	−2.16	1.61	−1.31	−1.81	−1.91	1.75	0.65	0.96	−1.87	2.32
BT_{11}–$BT_{6.7}$	44.93	41.10	50.06	41.44	26.22	44.53	37.77	39.89	8.10	23.66	18.29	35.24	0.80
$BT_{3.9}$–$BT_{3.7}$	−0.94	−2.20	−1.65	−2.24	−7.40	−2.85	−7.64	−6.61	−14.03	−9.24	−12.33	−10.81	−20.81
BT_{11}–$BT_{3.7}$	−3.17	−4.11	−10.01	−4.62	−25.22	−12.58	−19.58	−16.93	−26.32	−24.38	−32.64	−26.28	−37.19
BT_{12}–BT_{4}	−0.12	1.19	−5.92	0.62	−15.42	−7.41	−7.38	−6.14	−9.65	−11.84	−16.28	−9.04	−12.13
$BT_{13.7}$–BT_{14}	7.88	7.61	8.27	8.41	4.34	7.19	7.76	7.76	2.27	4.07	4.00	7.66	0.59
BT_{11}–$BT_{3.9}$	−2.23	−1.91	−8.35	−2.38	−17.82	−9.73	−11.94	−10.31	−12.28	−15.14	−20.31	−15.47	−16.38

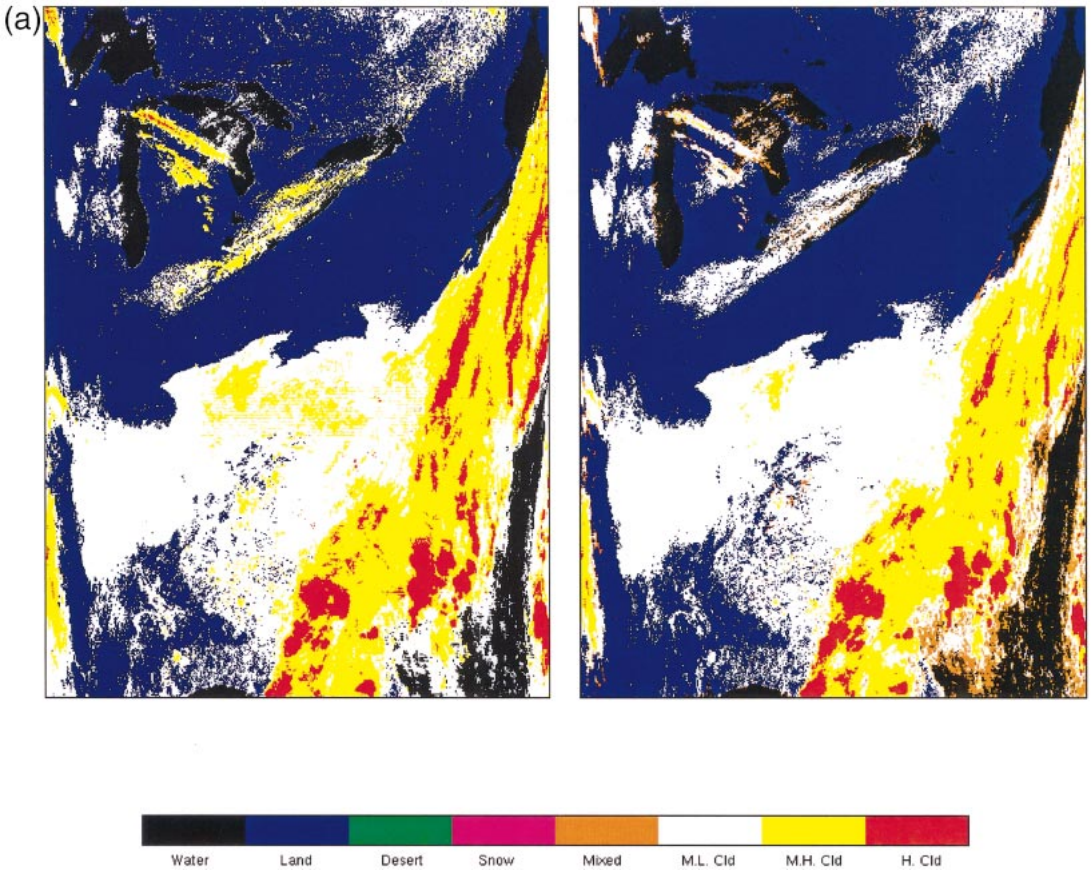

FIG. 3. (a) (left) MODIS cloud mask and (right) ML classification mask. Time is 1635 UTC 5 Sep 2000 for case 1. Classes of clear water, clear land, mixed types, middle-to-low clouds, middle-to-high clouds, and high clouds classified by the MODIS cloud mask and ML classification algorithms are indicated.

3) Update the mean vector and covariance matrix of each class after all pixels have been reassigned to the nearest classes.
4) Repeat steps 2 and 3 until convergence criteria are met. In this paper, if the sum of the off-diagonal elements for each class in the classification matrix (see the definition of classification matrix in section 7) is less than 6%, the iterations end. In general, approximately 6 to 7 iterations are needed for a final ML classification result.

4. Feature selection for MODIS surface and cloud-type classification

There are three types of features (radiances, variances of radiances, and spectral brightness temperature differences) in the MODIS classification. All the features are determined at 1-km resolution. More spectral bands are used for surface and cloud-type classification than used for cloud masking.

a. Spectral band radiances

Radiances provide the primary spectral information for different scene and cloud types. MODIS VIS/NIR bands 1–7, bands 17–29, and bands 31–35 are used in the daytime classification. The images for VIS/NIR bands 1–7 are all mapped into the IR spatial resolution of 1 km. Hereinafter, we use a GIFOV to define the MODIS original resolution; for example, for band 1 or 2, one GIFOV has 0.25-km resolution; for bands 3–7, one GIFOV has 0.5-km resolution; and for bands 17–36, one GIFOV has 1-km resolution. We use a pixel as the 1-km average of GIFOVs for VIS/NIR bands 1–7 images; for bands 17–36, a pixel is simply a GIFOV.

VIS/NIR bands 1–7 are known to be sensitive to various types of clouds. The IR shortwave bands 20–25 have a strong cloud reflective radiance component in addition to a thermal emission during the daytime. The IR midwave bands 27–29 can be used with longwave window bands 31 and 32 to detect clouds through their strong water vapor absorption effects. The IR longwave

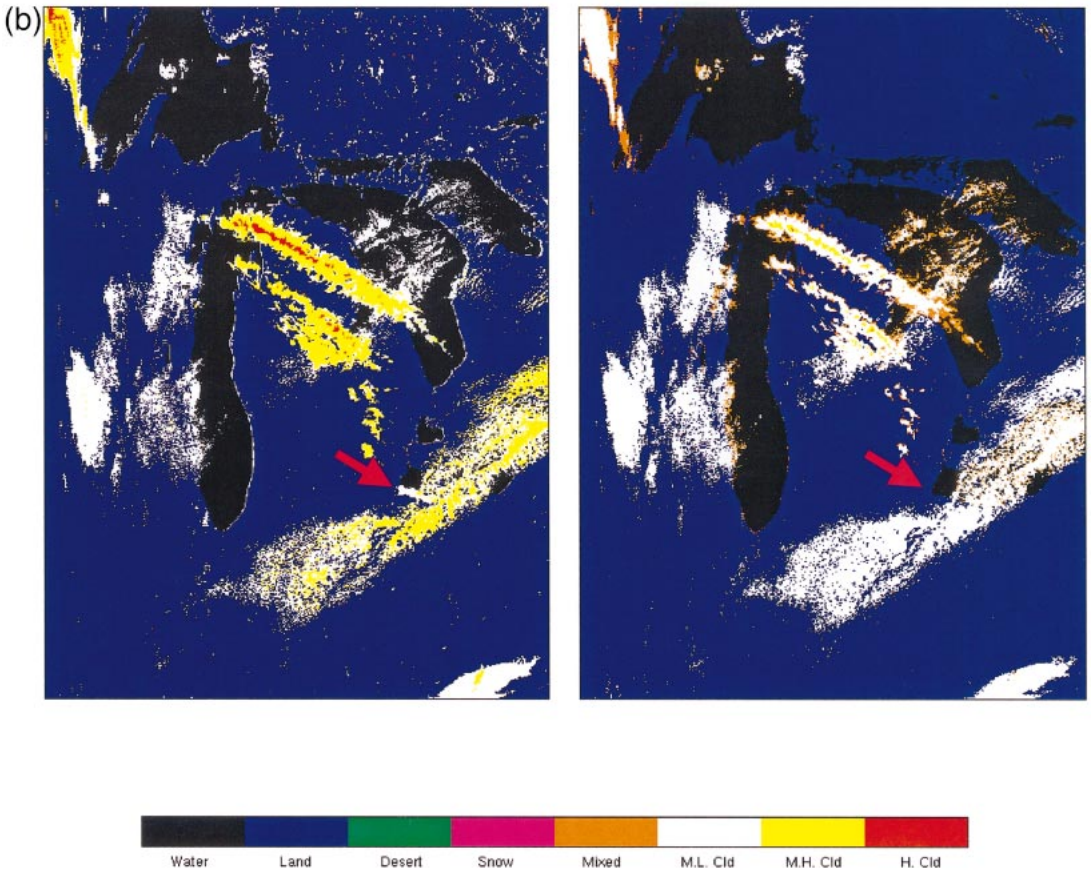

FIG. 3. (*Continued*) (b) Enlarged image of a portion of (a) that shows the benefit of the ML classification in the vicinity of the coastline (see arrows).

spectral bands 31–36, sensitive to different layers of clouds, are used to determine the cloud-top pressure (CTP) and effective cloud amount (ECA; Frey et al. 1999; Li et al. 2001b).

b. Variance images

A variance image is constructed for each of the VIS/NIR bands 1–7 images and for the IR longwave 6.7- (band 27), 7.3- (band 28), and 11-μm window (band 31) images. In the variance images for VIS/NIR bands 1–7, the value attributed to each 1-km pixel is the local standard deviation (LSD) of GIFOVs within the 1-km area [e.g., the standard deviation is computed from 4 by 4 values (GIFOVs) for bands 1 and 2, and from 2 by 2 GIFOVs for bands 3–7]. In the IR 6.7-, 7.3-, and 11-μm variance images, the value attributed to each pixel is the local standard deviation in the 3 by 3 GIFOV neighborhood of the pixel (the standard deviation computed from the nine values centered on the pixel). Variance images for VIS/NIR bands 1–7 along with variance images for IR bands 27, 28, and 31 are used in the ML classification procedure.

Variance or texture images of AVHRR have been used in detecting surface types and different types of clouds (Coakley and Bretherton 1982; Seze and Desbois 1987; Uddstrom and Gray 1996). In the associated IR 11-μm window variance image, the boundaries of different classes, or broken clouds, are well defined by very high variances, whereas the variance is far smaller inside a class. Cirrus corresponds to areas of high variances and low stratiform clouds to areas of low variances. In the associated VIS/NIR band 1 and band 2 images, edges of different classes still present large variances; however, contrary to the IR 11-μm window variances, low variances in VIS/NIR band 1 and band 2 are associated with cirrus clouds and relatively high variances with low stratiform clouds. Figure 1 (left) shows the MODIS 0.86-μm (band 2) image in units of reflectance (percent) and (right) its variance image at 1635 UTC on 5 September 2000 over the eastern part of the United States. High variances in Fig. 1 indicate cloud edges or low clouds. Figure 2 (left) shows the associated IR 11-μm window brightness temperature (K) and (right) its variance image. High variances in Fig. 2 indicate mixed clouds or cirrus clouds. The variance range approximately from 0% to 10% for VIS/NIR images and 0 to 6 K for IR images.

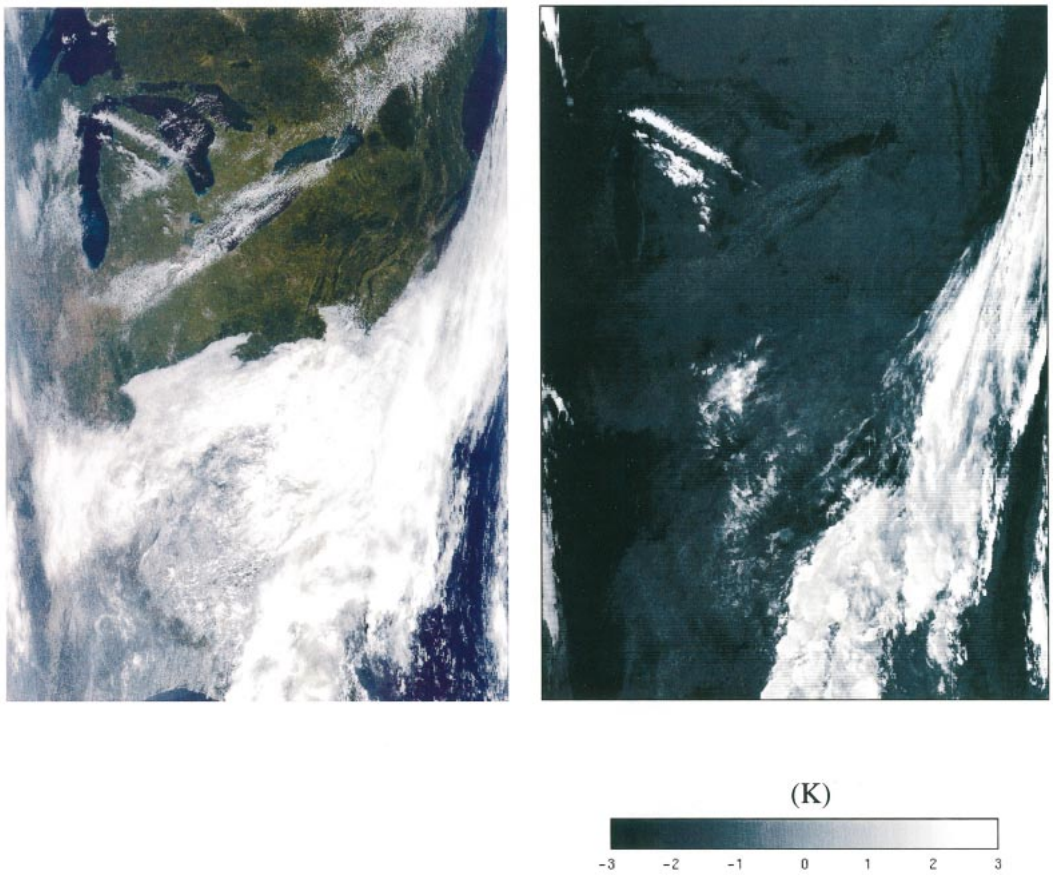

FIG. 4. (left) MODIS composite true color image from bands 1, 4, and 3 and (right) the $BT_{8.6} - BT_{11}$ image. Time is 1635 UTC 5 Sep 2000 for case 1.

c. Brightness temperature differences

Studies show that brightness temperature (BT) differences between two IR spectral bands are very useful for detecting clouds (Ackerman et al. 1998). For example, in the 8-μm region, ice/water particle absorption is at a minimum, while atmospheric water vapor absorption is moderate. In the 11-μm region, the opposite is true; particle absorption is at a maximum and atmospheric water vapor absorption is relatively minimal.

By using bands in these two regions in tandem, cloud properties can be distinguished (Inoue 1985; Prabhakara et al. 1993). Large positive $BT_{8.6} - BT_{11}$ values indicate the presence of cirrus clouds, where $BT_{8.6}$ defines the BT at 8.6 μm. This is due to the larger increase in the imaginary index of refraction of ice over that of water. For clear conditions, $BT_{8.6} - BT_{11}$ will usually be negative due to stronger atmospheric water vapor absorption at 8.6 μm than at 11 μm. Most clouds appear as positive values in the $BT_{8.6} - BT_{11}$ image.

A third band in the 12-μm region will enable cloud phase delineation (Strabala et al. 1994). Water particle absorption increases more between 11 and 12 μm than between 8.6 and 11 μm, while the increase of ice particle absorption is greater between 8.6 and 11 μm than between 11 and 12 μm. Thus, the $BT_{11} - BT_{12}$ values of water clouds are greater than the $BT_{8.6} - BT_{11}$. Conversely, $BT_{8.6} - BT_{11}$ values of an ice cloud scene are greater than coincident $BT_{11} - BT_{12}$. Therefore, ice and water clouds will separate in a scatter diagram of $BT_{8.6} - BT_{11}$ versus $BT_{11} - BT_{12}$, with ice clouds lying above the unity slope and water clouds below. Mixed phase or partial radiometer-filled ice over water clouds will exhibit characteristics of both ice and water clouds in this format, grouping near the unity slope. This information is extremely useful for nighttime classification when the visible measurements are not available.

Table 3 lists three types of features in the spectral information (reflectance and BTs), spatial information (variances), and BT differences used by the ML classification algorithm.

5. Identification of each class in the ML classification mask

Each class is identified based on the spectral and spatial radiance characteristics. In general, ML clas-

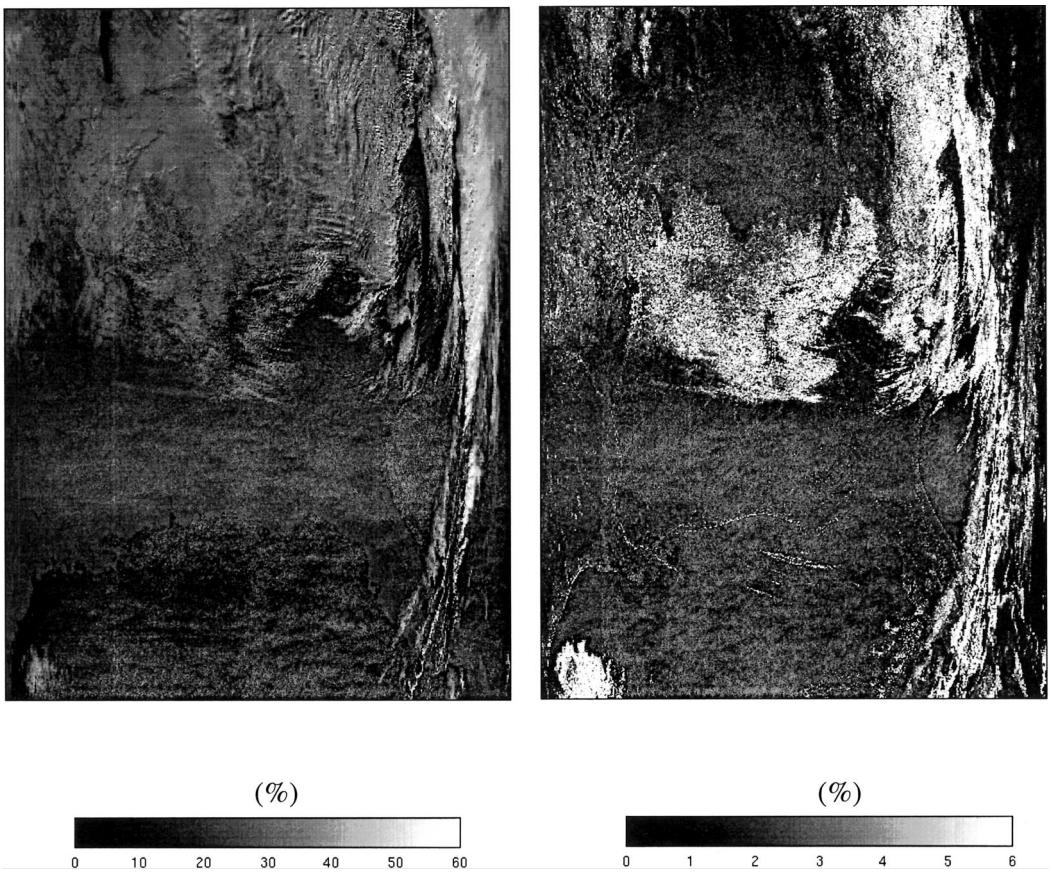

FIG. 5. (left) MODIS band 2 image and (right) its variance image. Time is 1640 UTC 17 Dec 2000 for case 2.

sifies most surface and cloud types with the same characteristics as the MODIS cloud mask (see Table 2 for the initial classes), although there might be significant adjustments in pixel assignments among classes. Some classes may change their physical characteristics after the ML classification procedure; for example,

- class 2–clear coast may change to another clear surface; or
- class 6–shadow of cloud may change to mixed surface type; or
- class 9–cirrus cloud may change to clear surface.

The cloud type in the MODIS cloud mask may also change after ML classification. For example, high cloud in the cloud mask changes to middle–high cloud when there is a substantial error in the MODIS cloud mask procedure. Several tests are applied to the class center values (VIS/NIR bands 1–7 reflectance; VIS/NIR bands 1–7, IR bands 27–28 and IR 11-μm variances; IR bands 20–25 and IR bands 27–35 brightness temperatures; as well as BT differences between two spectral bands) to ensure the identification. The tests include the three following steps.

a. First step: The identification of all clear surface types

Classes 1, 2, 4, and 7 are clear classes according to the MODIS cloud mask; however, they will need to pass two additional tests discussed below. Class 3 will be tested for desert or low clouds, class 5 will be tested for snow or low clouds, and class 9 will be tested for cloudy or clear. A class is determined to be clear only if it passes all the clear tests. Several tests are described below.

1) RADIANCE THRESHOLD AND SPECTRAL BRIGHTNESS TEMPERATURE DIFFERENCE TESTS

The clear tests used in the MODIS cloud mask algorithm are used to check each class of the ML classification. For example, during the daytime the difference $BT_{11} - BT_{3.7}$ becomes large and negative because there is reflection of solar energy at 3.7 μm. This technique is very successful at detecting low-level water clouds during the daytime. For details of the clear test procedures, see Ackerman et al. (1998). Only those classes passing all the clear tests continue to the variance image test.

TABLE 5. Class center values of 11 classes at 1640 UTC 17 Dec 2000 (case 2). Units and definitions as in Table 4.

Features	Water	Land	L. Cld	Land	Snow	Undecided	M.H. Cld	Land	H. Cld	M.L. Cld	M.H. Cld
Percentage	21.46	3.80	4.14	11.53	15.12	0.21	5.92	11.30	5.57	14.15	6.77
Class index	1	2	3	4	5	6	8	9	10	12	13
BAND 1	3.01	9.71	11.22	4.36	22.86	15.99	25.85	5.20	37.60	27.18	20.13
BAND 2	1.69	12.26	12.42	11.07	25.13	15.99	28.82	11.09	39.45	29.90	23.09
BAND 3	8.47	13.09	15.57	7.15	25.72	20.13	28.42	8.58	40.44	29.67	22.83
BAND 4	4.93	10.28	12.38	5.22	22.82	16.60	26.04	6.07	37.08	26.89	20.19
BAND 5	1.09	11.16	12.54	13.80	16.74	13.33	27.54	13.16	33.92	27.03	21.74
BAND 6	0.93	7.36	11.30	10.50	7.39	8.69	22.06	9.54	18.85	21.37	16.19
BAND 7	0.68	4.49	8.02	5.54	3.97	5.72	14.87	5.10	12.21	15.32	11.39
LSD–BAND 1	0.17	2.15	3.99	0.66	2.03	2.27	7.66	0.63	1.06	1.82	3.34
LSD–BAND 2	0.20	2.82	4.67	1.12	2.05	2.52	8.64	1.07	1.16	2.11	3.86
LSD–BAND 3	0.10	1.25	2.38	0.20	1.16	1.64	5.30	0.20	0.85	1.04	2.20
LSD–BAND 4	0.12	1.41	2.67	0.30	1.30	1.73	5.88	0.28	0.86	1.15	2.39
LSD–BAND 5	0.16	1.92	3.25	0.98	0.90	1.85	6.37	0.82	1.09	1.45	2.93
LSD–BAND 6	0.15	1.53	3.26	1.28	0.55	1.41	5.82	0.87	0.62	1.37	2.91
LSD–BAND 7	0.13	1.14	2.59	0.95	0.42	0.99	4.26	0.60	0.52	1.14	2.40
BAND 17	1.24	10.36	9.64	10.34	21.16	12.86	25.51	10.22	38.01	26.31	20.64
BAND 18	0.62	5.88	4.32	6.16	12.01	9.40	15.37	5.97	34.86	16.07	13.11
BAND 19	0.81	7.59	6.14	7.85	15.43	10.58	19.21	7.69	36.20	20.03	16.06
BAND 20	294.79	279.93	298.61	286.72	266.25	284.60	294.43	279.06	267.89	292.38	288.51
BAND 21	293.22	275.87	293.33	285.07	262.92	280.10	283.99	276.80	253.43	279.36	277.06
BAND 22	293.27	274.70	293.27	284.16	261.05	278.52	283.19	276.17	246.69	278.18	275.98
BAND 23	288.94	270.92	288.02	280.91	258.70	274.84	276.14	272.79	240.10	269.83	268.70
BAND 24	252.12	243.25	248.40	249.37	239.04	242.95	243.99	244.75	224.47	240.62	240.48
BAND 25	270.33	256.17	266.52	265.24	248.20	256.94	256.42	258.51	222.66	249.97	250.04
BAND 26	0.07	0.66	0.50	0.54	1.30	4.83	1.92	0.47	22.65	1.98	2.57
BAND 27	253.48	245.07	248.62	252.59	239.79	244.29	248.18	246.79	220.95	243.78	243.06
LSD–BAND 27	0.37	0.42	0.44	0.30	0.34	9.29	0.35	0.32	0.82	0.30	0.40
BAND 28	267.26	255.15	262.43	264.27	249.61	254.57	257.28	258.01	223.00	251.71	220.56
LSD–BAND 28	0.30	0.64	0.43	0.23	0.30	11.80	0.46	0.19	0.87	0.24	0.70
BAND 29	288.10	268.60	283.55	279.92	256.63	270.14	267.63	271.89	225.22	258.10	258.43
BAND 31	291.66	269.30	285.64	281.47	256.63	270.36	268.89	273.16	222.58	259.26	258.24
LSD–BAND 31	0.26	2.12	1.69	0.57	0.59	18.32	1.81	0.50	1.14	0.52	1.95
BAND 32	290.79	268.78	284.57	281.45	256.28	269.06	268.41	273.29	221.76	259.17	257.28
BAND 33	269.13	255.56	264.32	265.01	248.85	254.16	256.23	258.84	219.66	250.64	248.89
BAND 34	254.98	246.68	252.01	253.61	242.65	244.51	247.62	249.01	218.52	244.07	242.80
BAND 35	246.68	240.46	243.88	245.79	237.71	238.38	241.17	241.96	218.33	239.26	237.86
BT_{11}–BT_{12}	0.77	0.48	1.01	−0.06	0.35	0.99	0.50	−0.11	0.85	0.15	0.99
$BT_{8.6}$–BT_{11}	−2.51	−0.71	−2.12	−1.64	0.01	−0.66	−1.24	−1.17	2.65	−1.01	0.19
BT_{11}–$BT_{6.7}$	37.70	23.80	37.15	28.94	17.05	27.21	20.99	26.43	1.67	15.40	15.16
$BT_{3.9}$–$BT_{3.7}$	−1.34	−5.76	−5.06	−2.62	−5.32	−5.66	−10.71	−3.03	−21.15	−14.05	−12.61
BT_{11}–$BT_{3.7}$	−2.61	−12.08	−12.26	−5.14	−9.71	−12.65	−24.25	−6.00	−45.14	−32.96	−30.62
BT_{12}–BT_{4}	1.16	−2.69	−3.11	0.72	−2.36	−4.38	−7.29	0.37	−18.29	−10.64	−11.67
$BT_{13.7}$–BT_{14}	8.64	6.19	8.14	7.92	5.08	6.50	6.46	6.91	0.21	5.15	4.86
BT_{11}–$BT_{3.9}$	−1.27	−6.32	−7.20	−2.52	−4.39	−6.99	−13.53	−2.96	−23.99	−18.91	−18.02

2) VARIANCE IMAGE TESTS

The empirical interpretation of the variances can be summarized as (a) low VIS/NIR bands 1–7 variances and low IR 11-μm variances correspond to surface or homogeneous thick clouds; (b) relatively low VIS/NIR bands 1–7 variances, and high IR 11-μm variances correspond to cirrus over surface; (c) relatively high VIS/NIR bands 1–7 variances and low IR 11-μm variances correspond to quasi-total coverage by middle–low clouds; (d) high VIS/NIR bands 1–7 and IR 11-μm variances with correlated variations, correspond to mixed coverage by thick high and middle clouds. Using this interpretation, IR 11-μm variances and VIS/NIR bands 1–7 variances allow the distinction between partial broken clouds, semitransparent clouds, and surfaces that could not be separated in IR–VIS/NIR images (Seze and Desbois 1987). The combination of spectral (IR 11-μm window and VIS/NIR) and spatial (LSD of VIS/NIR bands 1–7 and IR 11-μm window) information may allow a better determination of the surface and cloud types. When the clouds form homogeneous layers, they produce partial coverages of the pixel or present local variations in the optical properties.

b. Second step: The identification of surface types for clear classes

This relies mainly on VIS/NIR bands 1 and 2 reflectance and VIS/NIR bands 1–7 variance information.

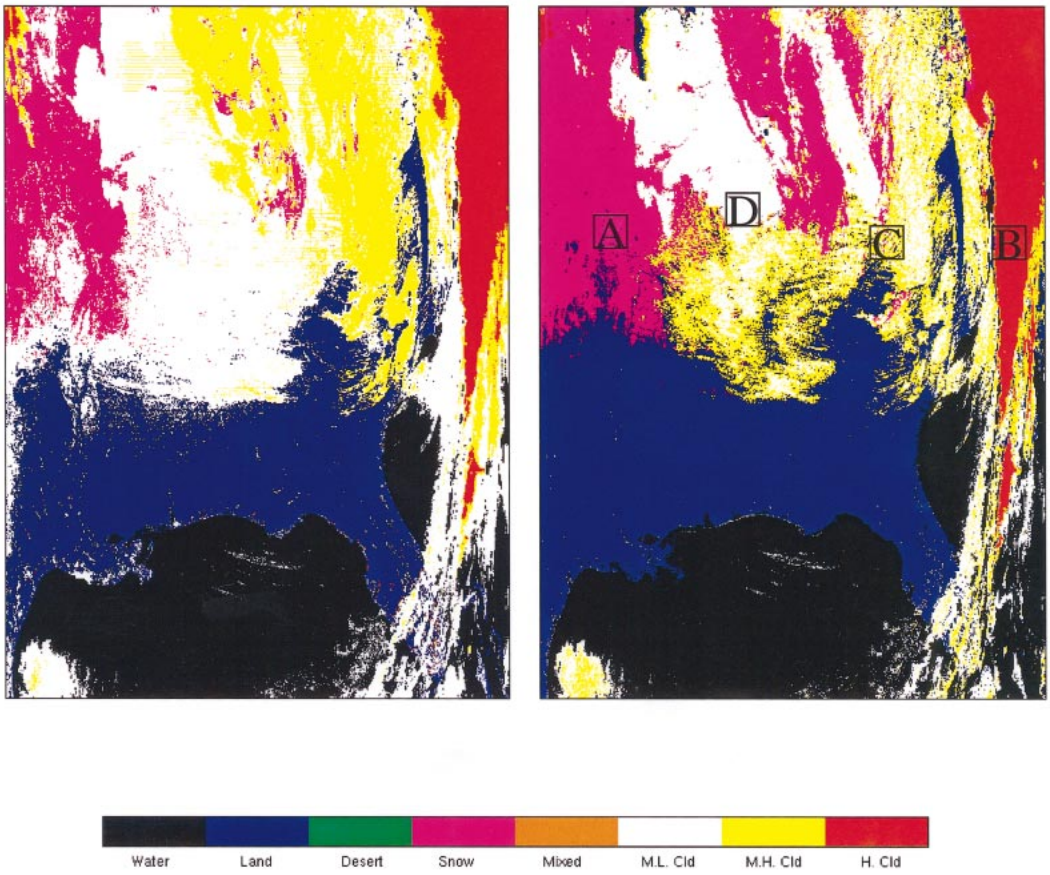

FIG. 6. (left) MODIS cloud mask and (right) ML classification mask. Time is 1640 UTC 17 Dec 2000 for case 2. The four boxes in the right-hand panel represent four classes for scatterplots in Fig. 8.

- Clear water class: band 2 has low reflectance, while band 1 has relatively high reflectance. Very homogeneous in bands 1–2 and IR 11-μm variance images.
- Clear land class: low bands 1 and 2 reflectance, also homogeneous in bands 1 and 2 variance images.
- Clear snow or ice class: high bands 1 and 2 reflectance, relatively low bands 6 and 7 reflectance, very homogeneous in all VIS/NIR bands 1–7 and IR 11-μm variance images.
- Desert class: relative high reflectance in all VIS/NIR bands 1–7 images, also very homogeneous in most VIS/NIR bands 1–7 images and IR 11-μm window image.
- Coastal class: low bands 1 and 2 reflectance; relatively high variance in bands 1 and 2 variance images, as well as in the IR 11-μm variance image.

c. Third step: The identification of cloud types (e.g., low/middle/high clouds)

The identification is based on the VIS/NIR bands 1–2 reflectance and IR 11-μm window brightness temperatures, as well as the variance images in VIS/NIR bands 1–7 and IR 11 μm mentioned above. For example, thick high clouds correspond to high reflectance, low IR 11-μm window brightness temperatures, low VIS/NIR bands 1–7 variances, and low IR 11-μm variances. In contrast, the cirrus clouds correspond to relatively low VIS/NIR bands 1–7 variances and high IR 11-μm variances. In the IR 11-μm window image, high clouds are usually colder than the lower clouds.

6. ML classification with MODIS multispectral band measurements

Three cases are presented. Each case contains a granule of MODIS data (2030 by 1354 pixels from a 5-min satellite pass).

a. Case 1

MODIS NIR band 2 and IR 11-μm window images at 1635 UTC 5 September 2000 are presented in Figs. 1 and 2 (left panels), respectively. Each class is initially

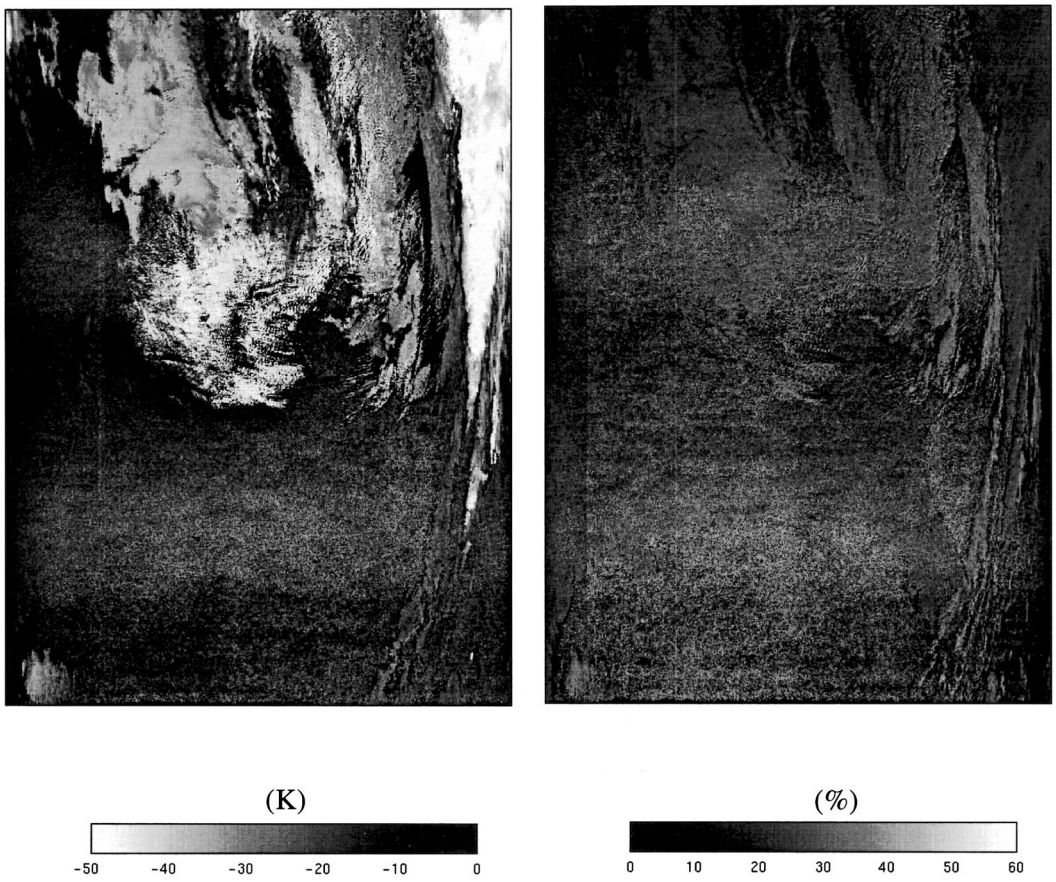

FIG. 7. (left) MODIS $BT_{11} - BT_{3.7}$ and (right) MODIS band 6 image. Time is 1645 UTC 17 Dec 2000 for case 2.

defined by the MODIS cloud mask algorithm (see Table 2 for the initial class index). The ML classification procedure ends after six iterations. Thirteen classes are obtained whose center values are given in Table 4. The identifications given to the classes are based on the previously described analysis.

Classes 1, 2, 3, and 4 correspond to clear surface: the most homogeneous, spatially, in VIS/NIR bands 1–7 and IR 11-μm window, warm in the IR 11-μm window, and dark in the VIS/NIR bands 1 and 2 images, negative values in $BT_{8.6} - BT_{11}$ image, and small values in the $BT_{11} - BT_{3.7}$ image.

Classes 5, 8, and 9 are mid-to-low clouds (''M.L. Cld'' in Tables 4–6) or mixed clouds: high IR 11-μm variances with very high variances in VIS/NIR bands 1–7, and large negative values in the $BT_{11} - BT_{3.7}$ image.

Class 6 corresponds to a class of mixed surface types (''Mixed'' in Tables 4–6): high variances in IR 11 μm and relatively low variances in VIS/NIR bands 1–7, warm in IR 11-μm window and dark in VIS/NIR bands 1 and 2 images, and small values in the $BT_{11} - BT_{3.7}$ image.

Classes 10 and 12 correspond to middle–high (''M.H. Cld'' in Tables 4–6): very bright in VIS/NIR bands 1 and 2 images, relatively low variances in VIS/NIR bands 1–7 and IR 11 μm, large negative values in the $BT_{11} - BT_{3.7}$ image, and relatively high reflectance in 1.38-μm image.

Class 13 corresponds to low clouds (''L. Cld'' in Tables 4–6): low variances in IR 11 μm with warm brightness temperature, high variances in VIS/NIR bands 1–7, very bright in VIS/NIR bands 1 and 2 images, and large negative values in the $BT_{11} - BT_{3.7}$ image.

Class 15 corresponds to high thick clouds (''H. Cld'' in Tables 4–6): relatively homogeneous in IR 11-μm window and VIS/NIR bands 1–7, coldest in IR 11-μm window and brightest in VIS/NIR bands 1 and 2 images, large negative values in the $BT_{11} - BT_{3.7}$ image.

Class 11 is an undecided class or mixed types: small percentage of pixels in the image, and huge variances in IR bands 27–28 and IR 11 μm.

Classes 7 and 14 were not found in this case.

Figure 3a shows the cloud mask (left) and classification mask (right). Using 15 unique colors in the display was not deemed practical for interpretation so we have combined the classes into eight types. In general,

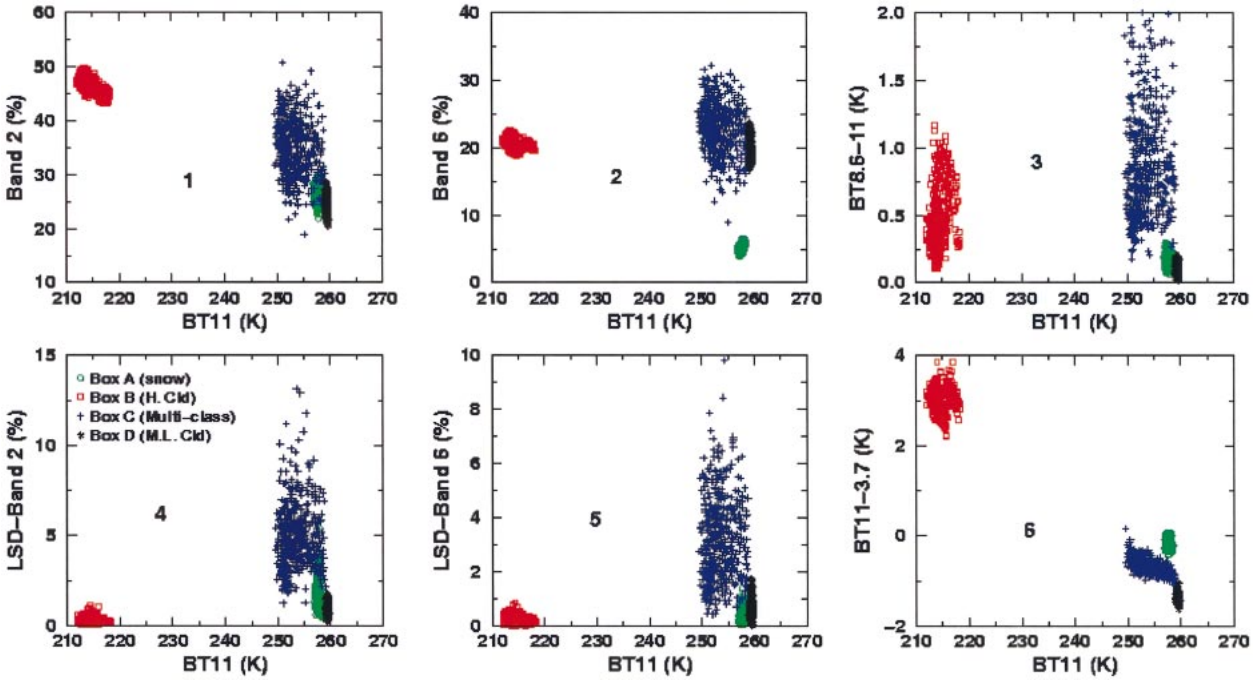

FIG. 8. Scatterplots of (panel 1) band 2, (panel 4) LSD band 2, (panel 2) band 6, (panel 5) LSD band 6, (panel 3) $BT_{8.6} - BT_{11}$, and (panel 6) $BT_{11} - BT_{3.7}$ vs IR 11-μm window brightness temperature for the four boxes outlined on the right panel of Fig. 6 (representing snow, low clouds, class of mixed cloud types, high clouds, from left to right, respectively). Panel numbers are located near the center of each panel.

the cloud mask and the classification mask have similar cloud–clear separations, however, the ML classification changes the cloud types of the initial classification obtained from the MODIS cloud mask. In addition, some water pixels in western Lake Erie, initially assigned to low clouds by the MODIS cloud mask algorithm, are classified as clear water by the ML classification, which can be clearly seen from the broad cloud mask and classification mask shown by Fig. 3b. This might be due to the relatively high VIS/NIR bands 1–2 reflectance of clear water pixels over that area, which are not well separated from the low clouds by the MODIS cloud mask algorithm. Another possibility is that the thresholds used in the cloud mask algorithm are not dynamic and they may not be indicative of the spectral characteristics over that area in this particular case. If the water scene and low clouds can be separated by some of those spectral and spatial characteristics, the ML classification process should be able to separate them.

Validation of cloud classification is always difficult (Rossow and Garder 1993). Two important steps in validation are image interpretation and quantitative analysis. Figure 4 shows the MODIS composite image from bands 1, 4, and 3 (left) and $BT_{8.6} - BT_{11}$ image (right). It shows the cloud pattern depicted in both images of Fig. 4 is well identified by both the MODIS cloud mask and ML classification mask in Fig. 3a.

b. Case 2

As the cloud mask algorithm is sometimes less reliable where snow cover exists, classification of a winter case is demonstrated here. Figure 5 shows the band 2 (left) and its variance (right) images for 1640 UTC 17 December 2000. In general, cloud and snow appear very similar in the 0.86-μm (band 2) image, even in the variance images for VIS/NIR bands 1–7. However, they appear dissimilar in the band 6 (1.64 μm) image. Eleven classes are obtained in this case whose class center values are given in Table 5. The identifications given to the classes are as follows.

Classes 1, 2, 4, and 9 are clear surface: very spatially homogeneous in the IR 11-μm window and VIS/NIR bands 1–7 images, warm in the IR 11-μm window and dark in VIS/NIR bands 1 and 2 images, and small values in $BT_{11} - BT_{3.7}$ image.

Class 3 is low clouds: relatively low variance in IR 11-μm window, brighter in the VIS/NIR bands 1 and 2 images than classes 2 and 9, and very high variances in VIS/NIR bands 1–7.

Class 5 corresponds to snow: very homogeneous in IR 11-μm window and VIS/NIR bands 6–7 images, bright in VIS/NIR bands 1 and 2 but relatively dark in bands 6–7 images, and small values in $BT_{11} - BT_{3.7}$ image.

Classes 8 and 13 correspond to middle–high clouds

or middle–low clouds: high variances in VIS/NIR bands 1–7 and IR 11 μm, bright in VIS/NIR bands 1 and 2 images, and large negative values in $BT_{11} - BT_{3.7}$ image.

Class 10 corresponds to high thick clouds: relatively homogeneous in both the IR 11-μm window and VIS/NIR bands 1–7 images, very cold in IR 11-μm window, very bright in VIS/NIR bands 1 and 2 images, and large negative values in $BT_{11} - BT_{3.7}$ image.

Class 12 corresponds to middle–low clouds: low variances in IR 11 μm, relative high variances in VIS/NIR bands 1–7 bright in the VIS/NIR bands 1 and 2 images and large negative values in $BT_{11} - BT_{3.7}$ image.

Class 6 is an undecided class or mixed types: small percentage of pixels in the image, with huge variances in IR bands 27–28 and IR 11 μm.

Classes 7, 11, 14, and 15 are not found in this case.

Figure 6 shows the associated MODIS cloud mask (left) and ML classification mask (right). In the cloud mask algorithm, snow is not well separated from the low clouds in the eastern part of the United States. However, it is well separated in the ML classification. Figure 7 shows the MODIS $BT_{11} - BT_{3.7}$ image (left) and 1.64-μm (band 6) image (right). Usually, clouds are revealed by large negative values in $BT_{11} - BT_{3.7}$ due to the strong solar reflection of the 3.7 μm over the clouds. However, the solar reflection of 3.7 μm over clear surfaces, even over the snow cover, is usually small. There are large negative values over the northeast coastal region and over the Lake Michigan area where clouds exist. The band 6 image also shows the cloud pattern in this area.

Figure 8 presents the scatterplots of band 2 (panel 1), LSD band 2 (panel 4), band 6 (panel 2), LSD band 6 (panel 5), $BT_{8.6} - BT_{11}$ (panel 3), and $BT_{11} - BT_{3.7}$ (panel 6) versus BT_{11} for the four boxes outlined in the right panel of Fig. 6 (representing snow, low clouds, class of mixed cloud types, and high clouds, respectively, from left to right). High clouds are well separated in panel 1; snow is well separated by band 6 in panel 2; all four objectives are well separated by $BT_{11} - BT_{3.7}$ image in panel 6. This figure illustrates that there is significant separation between snow and clouds in the ML classification procedure.

Figure 9 shows the snow cover map for 17 December 2000 from the National Oceanic and Atmospheric Administration (NOAA; available online at http://www.nohrsc.nws.gov/index.html). This snow chart was created from various sources of data including ground weather observations, Defense Meteorological Satellite Program (DMSP) microwave products, and other polar and geostationary satellite observations. Snow covers most of the northern United States; however, Lake Michigan was shown as open water in this chart, which is consistent with the ML classification results.

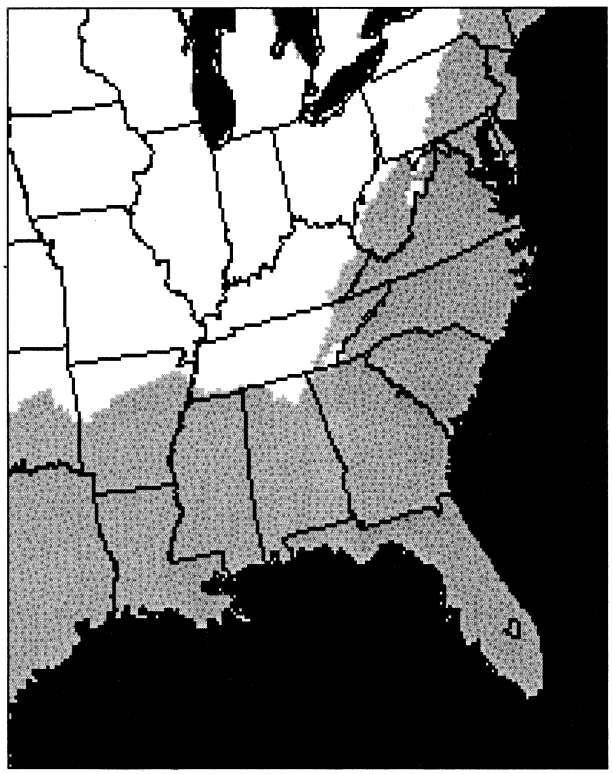

FIG. 9. NOAA's snow and ice chart on 17 Dec 2000. The white color is snow cover.

c. Case 3

The challenge of detecting clouds over desert region is the focus of case 3. Figure 10 shows band 2 (left) and its variance (right) images of an African Sahel/desert scene at 0935 UTC 5 November 2000, indicating clouds in the southern part of the image. The MODIS cloud mask algorithm sometimes has difficulties in desert areas since the VIS/NIR bands 1 and 2 reflectance is usually higher over clear desert than over other clear vegetated land, and sometimes clear desert is not well separated from low clouds in the MODIS cloud mask algorithm. Twelve classes are obtained from the cloud mask algorithm and the ML classification in this case; the class center values are given in Table 6. The identifications given to the classes are as follows.

Classes 1, 4, and 9 are clear surface: homogeneous in IR 11-μm window, dark in VIS/NIR bands 1 and 2 images, warm in IR 11-μm window image, and small values in the $BT_{11} - BT_{3.7}$ image.

Classes 2 and 3 are clear desert surface: very spatially homogeneous in IR 11-μm window and VIS/NIR bands 1–7 images, very warm in IR 11-μm window, relatively bright in most VIS/NIR bands 1–7 images, and small values in the $BT_{11} - BT_{3.7}$ image.

Class 8 corresponds to middle-to-low clouds: relatively bright in the VIS/NIR bands 1 and 2 images, low

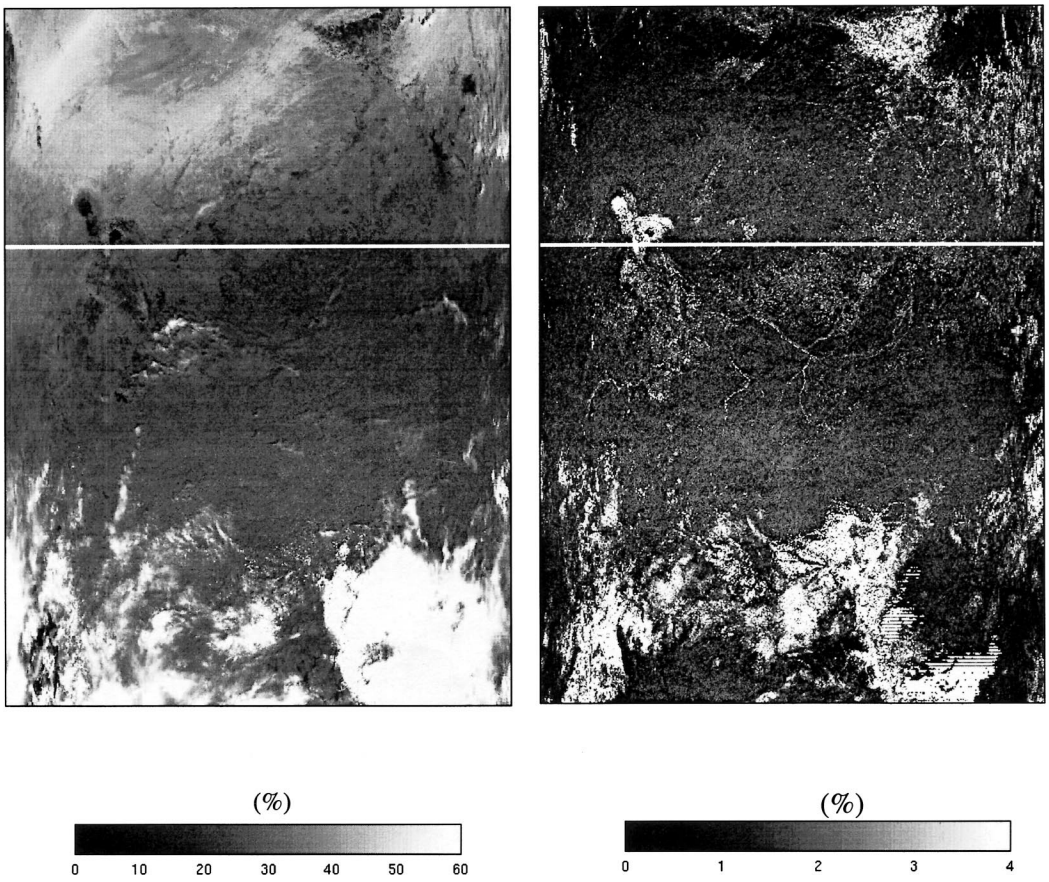

FIG. 10. (left) The MODIS band 2 image and (right) its variance image. Time is 0935 UTC 5 Nov 2000 for case 3.

variances in VIS/NIR bands 1–7, very high variances in IR 11-μm, and large negative values in the $BT_{11} - BT_{3.7}$ image.

Class 10 corresponds to high clouds: brightest in VIS/NIR bands 1 and 2 images, coldest in IR 11-μm window image, very homogeneous in VIS/NIR bands 1–7 images, relative high variances in IR 11 μm, and large negative values in the $BT_{11} - BT_{3.7}$ image.

Classes 11 and 12 correspond to middle-to-low clouds or middle-to-high clouds: bright in VIS/NIR bands 1 and 2 images, high variances in VIS/NIR bands 1–7, and IR 11 μm, and large negative values in the $BT_{11} - BT_{3.7}$ image.

Classes 13 and 15 correspond to middle-to-low clouds: bright in VIS/NIR bands 1 and 2 images, very high variances in VIS/NIR bands 1–7, relative high variances in IR 11 μm, and large negative values in the $BT_{11} - BT_{3.7}$ image.

Classes 5, 7, and 14 are not found in this case.

Figure 11 shows the MODIS cloud mask (left) and ML classification mask (right) for this case. In the MODIS cloud mask algorithm, a drought lake was misidentified (classified as clouds) but it is recognized by the ML classification (classified as water class in the right panel of Fig. 11). Some striped lines existed in the cloud mask due to the use of band 36 in the cloud mask algorithm; band 36 was not used in the ML classification. The cloud coverage from the cloud mask is very close to that of the ML classification results although there are significant cloud type changes (e.g., less high clouds in the ML classification than in the MODIS cloud mask). Also, the MODIS cloud mask has more clear desert area than the ML classification.

Figure 12 shows the MODIS $BT_{8.6} - BT_{11}$ image (left) and 11-μm image (right). Clouds indicate positive values in the $BT_{8.6} - BT_{11}$ image; large negative values in the $BT_{8.6} - BT_{11}$ image here should correspond to desert since the surface emissivity has the potential to be significantly lower at 8.6 μm than at 11 μm in desert regions (Salisbury and D'Aria 1992).

The initial classification results from the cloud mask may be sensitive to the thresholds in some regions, especially where desert exists. In order to test the sensitivity of both the MODIS cloud mask and ML classification algorithms to the thresholds used in the MODIS cloud mask, the thresholds were changed in the MODIS cloud mask algorithm. Some arid and semiarid zones were purposefully misidentified as vegetated land,

TABLE 6. Class center values of 12 classes at 0935 UTC 5 Nov 2000 (case 3). Units and definitions as in Table 4.

Features	Water	Desert	Desert	Land	Mixed	M.L. Cld	Land	H. Cld	M.H. Cld	M.L. Cld	M.L. Cld	M.L. Cld
Percentage	0.28	15.58	20.26	20.36	3.41	9.00	10.61	5.97	6.58	4.50	2.29	0.64
Class index	1	2	3	4	6	8	9	10	11	12	13	15
BAND 1	12.03	17.34	32.68	7.00	11.69	18.85	9.92	68.07	39.52	45.04	22.76	39.15
BAND 2	13.43	26.65	41.28	20.94	25.03	30.18	23.01	68.07	46.17	51.62	33.75	46.18
BAND 3	16.77	13.46	19.23	9.81	14.28	22.65	14.16	71.84	43.62	48.04	24.84	41.59
BAND 4	13.70	14.18	24.06	8.26	12.51	20.14	11.64	67.88	40.32	45.49	23.14	39.75
BAND 5	11.62	34.46	49.16	25.18	28.00	31.51	25.67	54.43	42.33	48.66	35.10	41.60
BAND 6	8.82	35.44	51.72	17.83	21.70	22.82	17.55	22.15	23.16	38.67	28.91	32.04
BAND 7	5.14	25.83	45.67	8.16	12.40	14.27	8.42	11.92	12.75	25.11	19.05	18.76
LSD–BAND 1	1.45	1.05	0.66	0.37	1.92	1.45	0.49	0.80	1.04	3.36	6.23	13.25
LSD–BAND 2	3.37	1.41	0.86	0.82	2.75	1.31	0.79	1.47	0.93	3.31	6.20	12.64
LSD–BAND 3	0.81	0.25	0.22	0.10	0.92	1.01	0.30	0.69	0.87	2.35	3.74	10.08
LSD–BAND 4	0.96	0.46	0.34	0.16	1.12	1.04	0.32	0.68	0.87	2.46	4.28	10.92
LSD–BAND 5	2.67	1.14	0.74	0.60	2.23	0.99	0.63	1.89	1.09	2.79	4.60	9.29
LSD–BAND 6	2.08	1.29	0.66	0.60	2.33	0.89	0.55	0.33	0.47	1.78	4.94	8.41
LSD–BAND 7	1.30	1.37	0.76	0.55	1.93	0.85	0.50	0.32	0.42	1.24	4.06	5.78
BAND 17	9.15	22.78	34.92	16.53	18.74	24.08	17.35	56.54	40.05	42.13	24.83	34.62
BAND 18	3.60	11.06	17.53	5.63	6.21	12.56	6.11	57.01	28.50	24.37	9.16	15.15
BAND 19	5.29	15.46	24.05	9.34	10.29	16.31	9.73	59.12	32.49	30.76	14.19	22.04
BAND 20	299.16	320.95	320.61	307.96	309.07	299.96	302.65	265.43	275.63	302.03	308.12	303.03
BAND 21	297.19	317.10	313.66	307.10	306.07	292.99	300.57	252.86	266.26	290.02	301.61	296.19
BAND 22	296.84	317.16	314.15	307.13	306.12	292.41	300.53	242.10	262.41	289.26	301.65	295.79
BAND 23	293.10	311.83	306.77	304.37	301.49	286.93	296.01	235.86	257.40	282.16	295.88	290.43
BAND 24	252.91	259.94	257.77	259.27	255.79	246.68	251.43	224.48	233.50	246.52	253.66	253.51
BAND 25	271.31	283.92	279.82	279.97	276.22	261.39	271.26	219.43	239.28	256.72	270.88	268.46
BAND 26	1.04	1.32	1.77	0.73	1.08	5.05	1.83	32.86	13.66	4.99	1.60	2.28
BAND 27	240.71	245.88	245.56	241.15	241.18	233.98	236.74	216.41	226.11	238.52	240.89	213.52
LSD–BAND 27	0.72	0.72	0.62	0.65	0.69	1.02	0.81	1.20	1.23	0.64	0.62	0.59
BAND 28	255.16	264.79	265.04	257.90	256.47	245.95	251.58	218.68	232.46	249.74	255.32	225.19
LSD–BAND 28	0.99	0.72	0.53	0.71	0.90	1.61	1.12	1.21	1.81	0.86	0.76	0.73
BAND 29	286.30	305.55	294.51	297.65	293.19	269.51	286.92	220.23	241.63	263.45	284.13	280.06
BAND 31	287.58	310.93	304.84	302.04	295.61	267.40	287.97	216.93	238.19	263.52	286.19	249.48
LSD–BAND 31	2.52	0.89	0.47	0.87	2.08	3.68	2.13	1.54	3.20	2.00	2.21	2.21
BAND 32	285.59	310.35	305.76	299.99	293.53	264.05	285.55	215.84	236.22	262.05	284.27	279.70
BAND 33	264.51	277.27	275.29	272.93	268.06	249.40	261.24	214.92	230.65	252.69	264.52	263.43
BAND 34	253.54	261.41	259.90	260.34	256.11	242.27	250.17	213.98	227.35	246.29	254.22	254.44
BAND 35	246.00	252.09	250.77	252.13	248.17	237.30	243.08	214.53	225.43	240.98	246.82	247.32
NDVI–vegetation*	152.19	182.78	167.65	225.37	207.45	186.21	212.30	152.97	162.89	162.16	183.76	171.29
NDVI–snow	187.88	85.55	94.85	95.66	109.70	141.94	119.87	225.18	189.46	159.87	130.99	156.94
BT_{11}–BT_{12}	1.93	0.52	−0.85	1.43	2.01	3.38	2.44	1.10	2.02	1.52	1.90	1.70
$BT_{8.6}$–BT_{11}	−1.34	−5.49	−10.05	−3.04	−2.46	2.13	−1.04	3.31	3.42	−0.05	−2.07	−1.18
BT_{11}–$BT_{6.7}$	46.86	65.24	59.13	59.91	54.45	33.19	51.20	0.59	12.31	25.23	45.35	40.51
$BT_{3.9}$–$BT_{3.7}$	−2.60	−3.79	−7.34	−0.92	−2.99	−7.61	−2.20	−23.27	−13.15	−12.68	−6.33	−6.65
BT_{11}–$BT_{3.7}$	−12.44	−9.98	−16.44	−6.63	−13.51	−32.71	−14.75	−48.37	−37.27	−38.33	−21.66	−20.79
BT_{12}–BT_{4}	−7.82	−1.40	−1.43	−3.69	−7.86	−22.96	−10.57	−19.78	−21.14	−20.10	−11.54	−10.73
$BT_{13.7}$–BT_{14}	7.52	9.49	9.23	8.70	7.95	4.95	7.06	−0.53	1.95	5.31	7.39	7.11
BT_{11}–$BT_{3.9}$	−9.83	−6.20	−9.10	−5.71	−10.52	−25.09	−12.55	−24.91	−24.12	−25.65	−15.33	−14.14

* NDVI is normalized difference vegetation index.

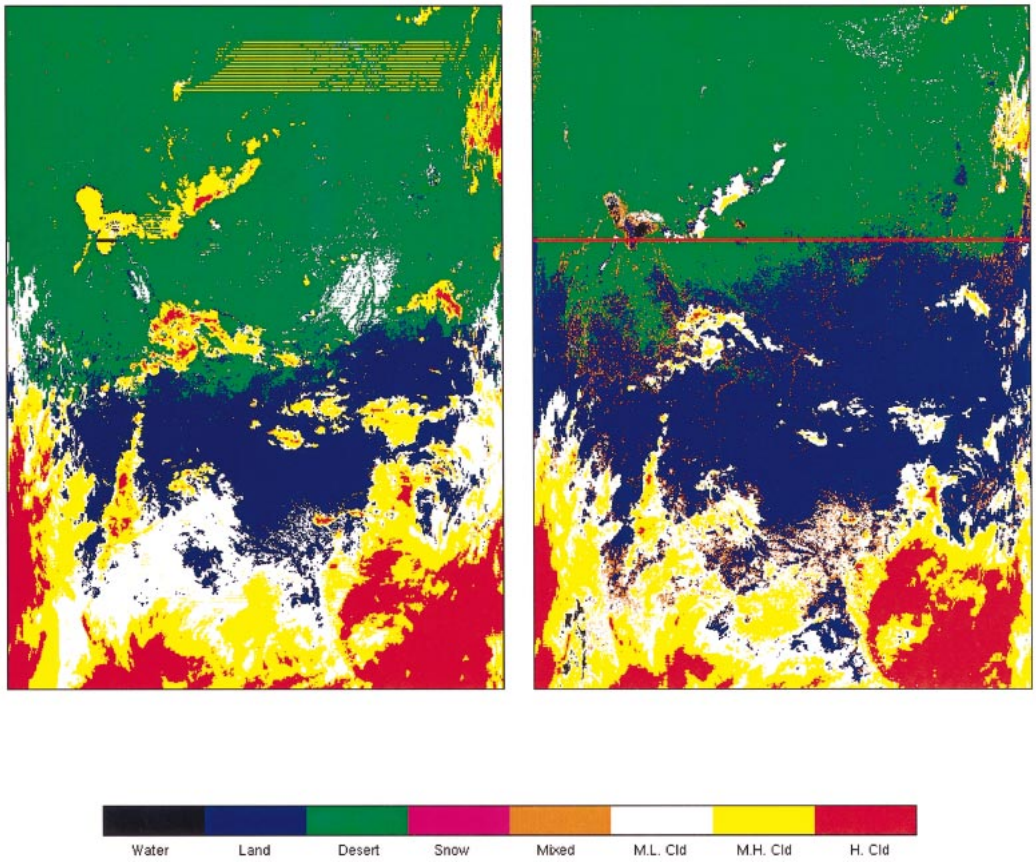

FIG. 11. (left) MODIS cloud mask and (right) ML classification mask. Time is 0935 UTC 5 Nov 2000 for case 3.

where visible band thresholds are lowered. The MODIS cloud mask then misinterpreted the brighter than expected surface reflectances as clouds. Figure 13 is the MODIS cloud mask (left) with altered (incorrect) thresholds and its corresponding ML classification mask (right). In the cloud mask algorithm, many desert pixels are mistaken for lower clouds due to inappropriate thresholds; however, those low cloud pixels are correctly reclassified as desert after the ML classification. Although there are some differences for the desert–land separation between the two classifications (see Figs. 11 and 13), the clear–cloud separation is almost the same in both classifications. This offers some reassurance that the ML classification procedure is relatively insensitive to the thresholds used in the MODIS cloud mask algorithm.

7. Discussion

Classification accuracy, computation efficiency, and separability of each class are very important considerations when applying this technique in the MODIS real-time data processing.

Classification accuracy is important, and several sources of errors should be addressed. First, a specific type of scene or cloud may not be classified or separated; this usually happens when the class appears very close to another class in the MODIS visible and infrared imagery. For example, snow sometimes appears very similar to low clouds and is difficult to separate; it may simply be misclassified as low clouds. Second, pixels at the boundaries between two different classes may be assigned to the wrong class. When pixels are close to two classes, those pixels are difficult to assign. Third, some classes may be incorrectly identified; this happens to some low cloud types. In general, clear scenes can be identified with considerable confidence since they are warmer in the IR window band, have lower reflectance in the visible bands, and are more homogeneous in the LSD images. Some ML classification errors can be reduced by using a more accurate initial classification or using more a priori knowledge. A better initial classification requires less adjustment for each class in the iterations and reduces the number of iterations, therefore producing more reliable final classification results. However, a poor initial classification requires more adjustments for each class and more iterations, therefore producing a classification result that might not be stable. In addition, instrument noise and calibration errors may affect the cloud mask algorithm, and thus the classifi-

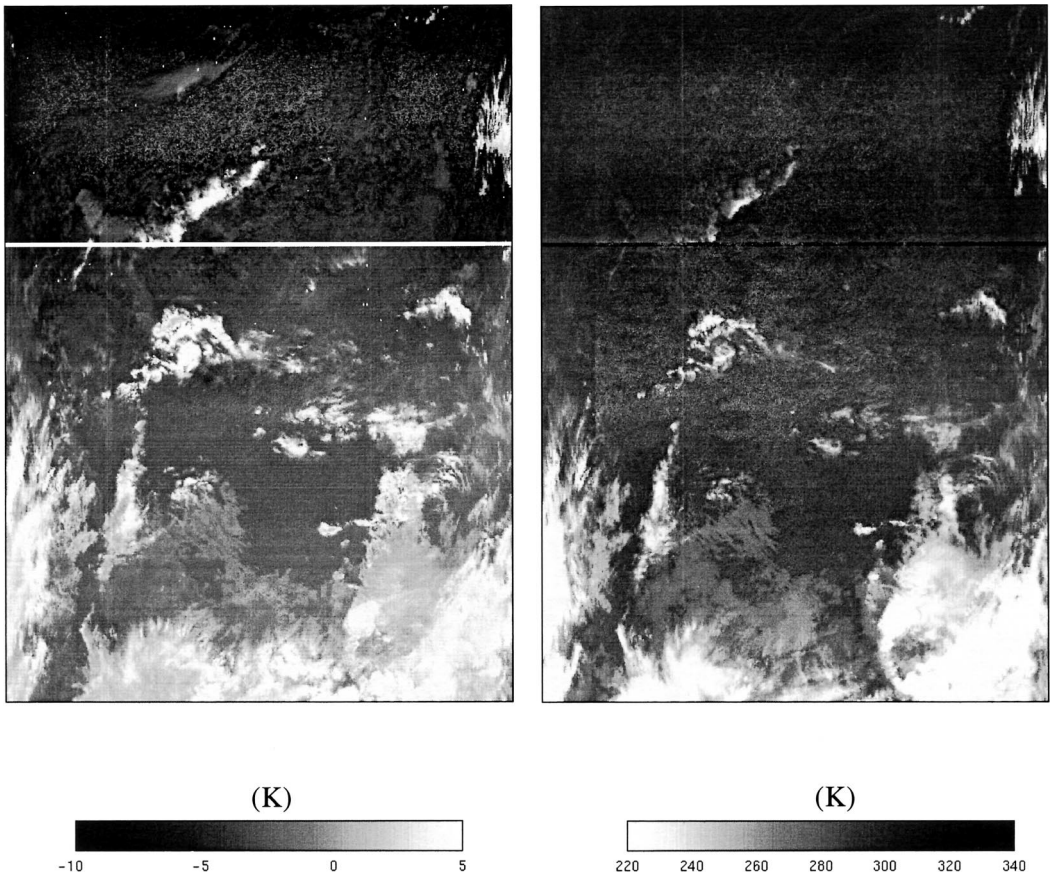

FIG. 12. (left) MODIS $BT_{8.6} - BT_{11}$ image and (right) 11-μm image. Time is 0935 UTC 5 Nov 2000 for case 3.

cation results. Accurate calibration is necessary to avoid errors in the cloud mask since the cloud mask algorithm uses a variety of thresholds. Mathematically, the iterative classification procedure is convergent; however, the convergence speed and stability are very dependent on initial classification, separability of different classes, selection of features, and definition of distances used to separate classes in the classification algorithm.

Computation efficiency is important for real-time data processing, as with MODIS data from a direct broadcast stations. The ML classification procedure for a MODIS granule takes several minutes on a Silicon Graphics, Inc., Origin 2000 computer or a Sun UNIX workstation. More iterations require more computation time, with the iteration number depending on the initial classification. A coarse initial classification—for example, a simple visible and infrared box classification (Li and Zhou 1990)—will need more iterations. A better initial classification, for example, one based on the cloud mask in this paper, needs fewer iterations for convergence. Determination of the iteration convergence is based on a classification matrix $\mathbf{C}(i, j)$ that indicates the percentage of pixels of the ith class of the last iteration assigned to the jth class after the current iteration. Figure 14 shows the classification matrix of the first iteration (Fig. 14a), the third iteration (Fig. 14b), and the sixth iteration (Fig. 14c) of case 1. It can be seen from Fig. 14 that there are significant changes from the first iteration to the third iteration, but the matrix tends to the diagonal after the sixth iteration indicating convergence in the classification procedure. Usually, six iterations produce stable classification results.

Separability is very important in the classification. In general, if two classes are separated by a spectral band or a spatial characteristic, they are separable in the classification. Figure 8 demonstrates that several classes have different spectral or spatial characteristics. In order to further analyze the separability of two different classes, the distance between each class and its neighbor class (a neighbor class is defined as its nearest class in terms of distance) is calculated. The distance between two classes ω_i and ω_j is defined by

$$D(\boldsymbol{\mu}_i, \boldsymbol{\mu}_j) = (\boldsymbol{\mu}_i - \boldsymbol{\mu}_j)^{\mathrm{T}} \boldsymbol{\Sigma}^{-1} (\boldsymbol{\mu}_i - \boldsymbol{\mu}_j), \qquad (4)$$

where $\boldsymbol{\Sigma}$ is the covariance matrix for all pixels. The uncertainty in the distance, or maximum noise distance, can be estimated by Eq. (4) as

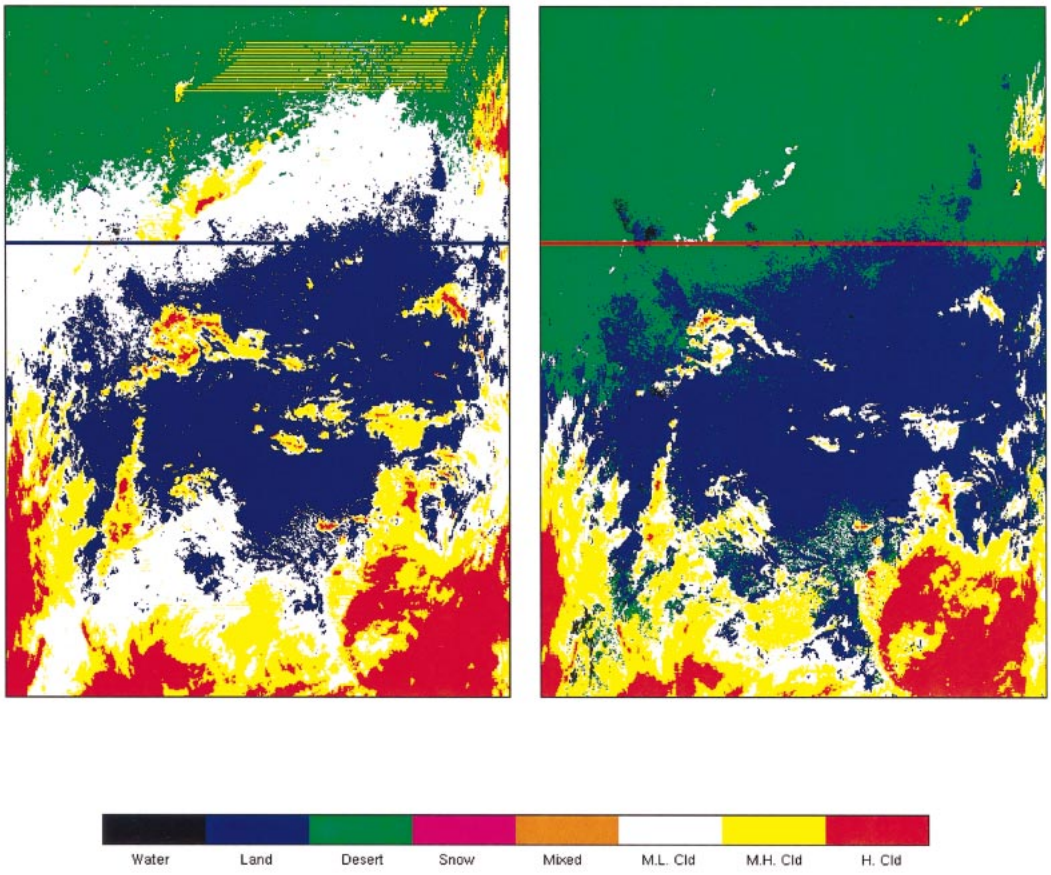

FIG. 13. (left) MODIS cloud mask with alternate (incorrect) thresholds and (right) its corresponding ML classification mask. Time is 0935 UTC 5 Nov 2000 for case 3. This figure is part of the sensitivity study.

$$\delta D(\boldsymbol{\mu}_i, \boldsymbol{\mu}_j) \le 4|\boldsymbol{\eta}^T \boldsymbol{\Sigma}^{-1}(\boldsymbol{\mu}_i - \boldsymbol{\mu}_j)|, \quad (5)$$

where $\boldsymbol{\eta}$ is the noise vector for each feature used in the ML classification. Figure 15 shows the distance between each class and its neighbor class, as well as the maximum noise distance based on the classification for case 1. In Fig. 15, for example, C2–C4 means that class 4 is the neighbor of class 2. From Fig. 15, most classes are well separated, but classes 2 and 4 are very close and thus not well separated (both class 2 and 4 are clear land in this example). In general, most classes from the classification procedure should be separable from each other. All classes should be separable since the class distances are all larger than the maximum noise distances. Note that the distance between a cloud class and its nearest clear neighbor class can also be used as a confidence level for this cloud class in ML classification. For example, if a low stratiform class is close to its nearest clear neighbor class, say snow class, then a low confidence level should be assigned to this cloud class.

Use of the variance images will improve the accuracy of ML classification. Figure 16 is similar to Fig. 6 but the ML classification mask in the right panel does not use VIS/NIR bands 1–7, IR bands 27–18, and IR band 31 variance images. More clouds are detected by ML classification in Fig. 16 in southern Florida when compared with the classification mask in Fig. 6, which includes all variance images. This might be due to the similar appearance of clouds and surface in that area in both VIS/NIR bands 1–2 and IR 11-μm window images, but they should have significantly different appearances in some of the variance images. In addition, some clear land pixels in southern Florida are classified as mixed surface type by ML classification without variance images, indicating that variance images play an important role in identifying some surface types. The classification matrix was computed to indicate the percentage of pixels in the *i*th class of ML classification with variance images assigned to the *j*th class of ML classification without variance images. It shows that class 5 of snow has almost no change, indicating that the snow detection is less sensitive to the variance images. Some pixels of class 4 (clear land) in the ML classification with LSD have changed to class 6 (mixed surface types) in the ML classification without LSD (see Table 5 for the 11 classes).

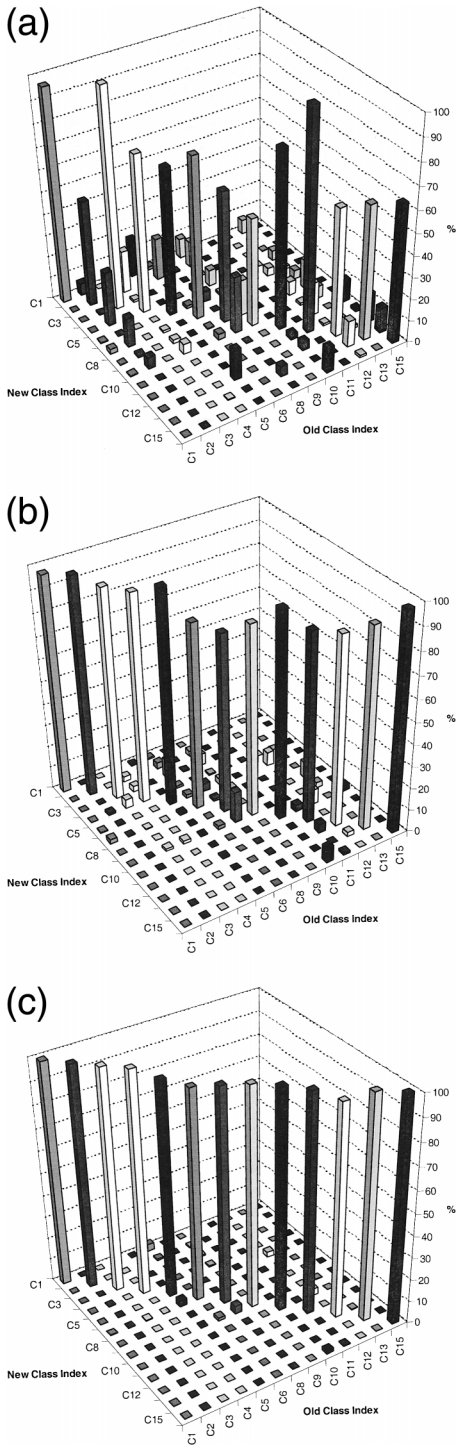

FIG. 14. MODIS ML classification matrix of (a) the first iteration, (b) the third iteration, and (c) the sixth iteration of case 1. Time is 1635 UTC 5 Sep 2000.

The size of the image can also influence the classification results. Currently, a granule of MODIS data (2030 by 1354 pixels) is used for a scene classification. On one hand, if the size of the image is too small, there might be fewer classes contained in the data and the separability might be low since there is no spatial variation in the imagery. On the other hand, if the size of the image is too large, there may be too many spatial variations in the imagery and too many classes so that different classes may show similar spectral or textural characteristics. A proper size is needed to allow enough scene variation but to avoid classifying different classes as one.

This ML classification procedure is pursued to extract the maximum information from MODIS measurements, to reduce the need for auxiliary data, and to have a better understanding of the clear-sky and cloud variability. If auxiliary data is not available or, in certain situations (such as in the presence of snow), the cloud mask may not be of good quality, a simple visible–infrared box classification can be used for initial classification (Li and Zhou 1990). Also, if the previous near-time classification center values were stored as training or reference data, these center values could also be used for initial classification based on the Bayesian decision method (Li et al. 1992).

8. Conclusions and future work

An ML classification initialized from the MODIS cloud mask algorithm was used to classify the scenes and clouds. The VIS/NIR and IR 1-km-resolution spectral information and VIS/NIR/IR spatial information are used in the classification. The aim of this paper is to demonstrate the usefulness of multiband spectral and spatial imagery information in identifying clear and cloudy scene types, and to find an effective way to improve the MODIS cloud mask when the thresholds used in the cloud mask algorithm are not representative. Results of applying reflectance, BT, local variances, and BT differences between two IR spectral bands confirm the usefulness of these parameters for cloud–clear separation, as well as for separating between the cloud types or clear types. The 1-km-resolution ML classification mask improves the 1-km-resolution MODIS cloud mask in some situations. Combined use of the MODIS cloud mask and ML cloud classification improves identification of clear skies in the MODIS imagery as well as cloud types.

Future work includes more case studies, especially in polar regions and African deserts where the surfaces may have a very unique appearance in the MODIS imagery. The utility of prior classification results as an initial classification will be studied; for example, daytime classification results can be used as the initial classification for nighttime classification since the cloud mask is less reliable at night. In addition, the impact of using classification in atmospheric profile and cloud retrievals will be studied. The size for image processing and its effect on cloud classification will also be investigated. Global classifications will also be investigated

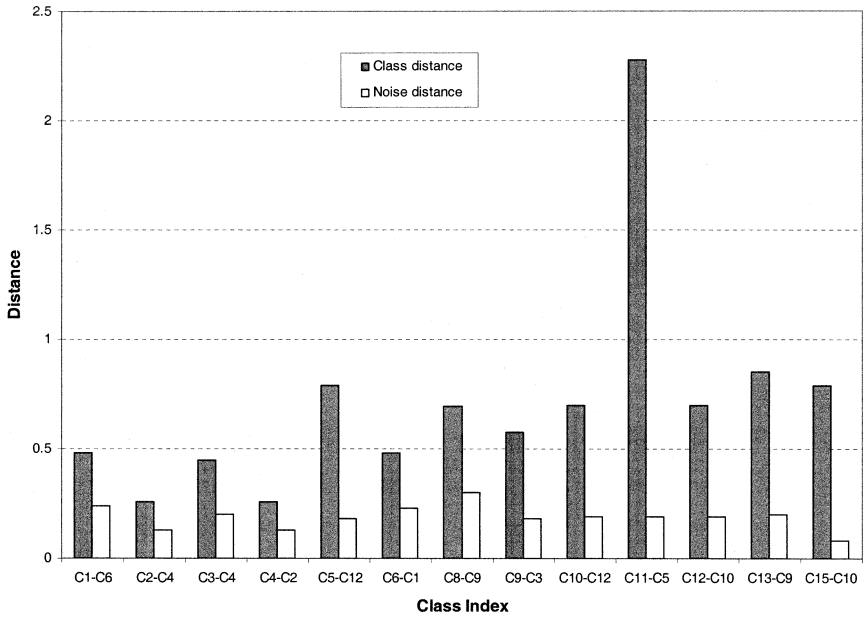

FIG. 15. Distance between each class and its neighboring class, along with the maximum noise distance based on the classification for case 1. Time is 1635 UTC 5 Sep 2000.

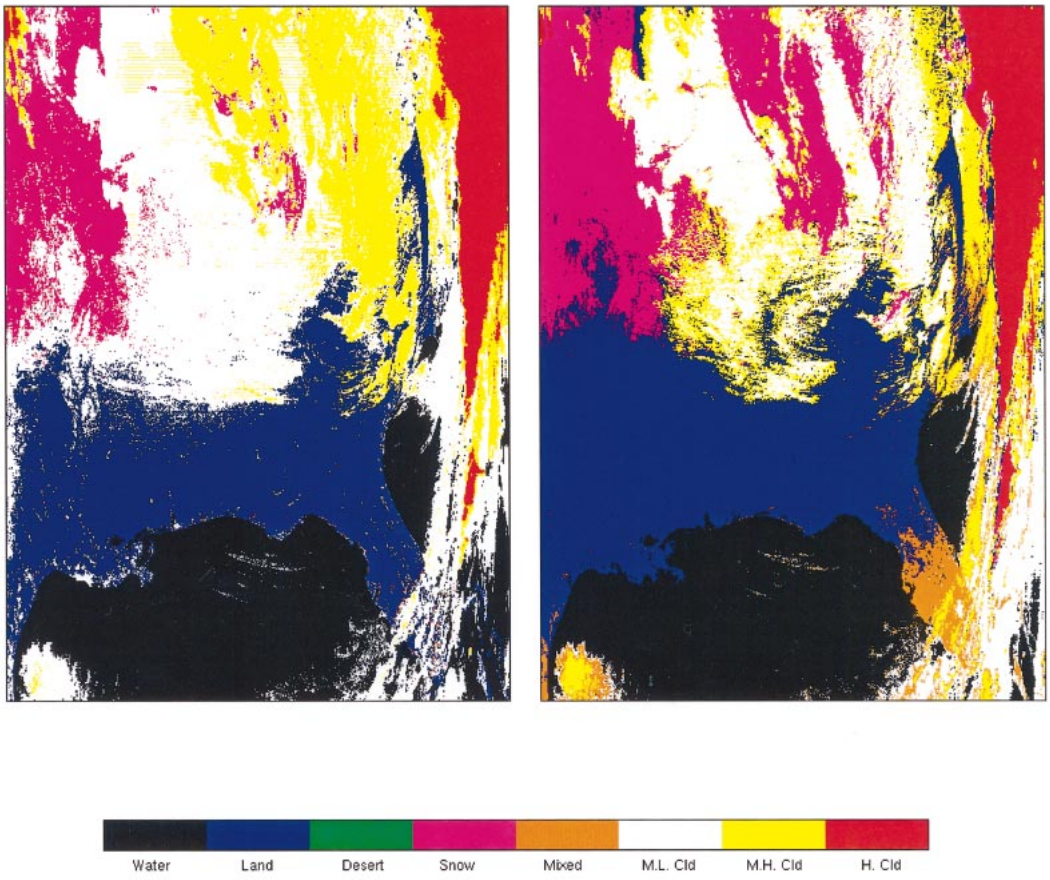

FIG. 16. (left) MODIS cloud mask and (right) ML classification mask without variance images for case 2. Time is 1640 UTC 17 Dec 2000.

and the maximum number of cloud classes will be explored.

Acknowledgments. The author thanks Dr. Xiangqian Wu for valuable discussions and suggestions regarding this work. Mr. Liam E. Gumley provided generous assistance in using the MODIS data. Three anonymous reviewers' comments were of considerable help in improving the text. This work was partly funded by NASA contracts relating to the International MODIS and AIRS Processing Package NAG5-9389, the MODIS Science Team NAS5-31367, and NOAA Advanced Baseline Imager Study NA07EC0676.

REFERENCES

Ackerman, S. A., K. I. Strabala, W. P. Menzel, R. A. Frey, C. C. Moeller, and L. E. Gumley, 1998: Discriminating clear sky from clouds with MODIS. *J. Geophys. Res.,* **103** (D24), 32 141–32 157.

Allen, R. C., Jr., P. A. Durkee, and C. H. Wash, 1990: Snow/cloud discrimination with multispectral satellite measurements. *J. Appl. Meteor.,* **29,** 994–1004.

Baum, B. A., and Q. Trepte, 1999: A grouped threshold approach for scene identification in AVHRR imagery. *J. Atmos. Oceanic Technol.,* **16,** 793–800.

Coakley, J. A., and F. P. Bretherton, 1982: Cloud cover from high resolution scanner data: Detecting and allowing for partially filled fields of view. *J. Geophys. Res.,* **87,** 4917–4932.

Desbois, M., G. Seze, and G. Szejwach, 1982: Automatic classification of clouds on Meteosat imagery: Application to high-level clouds. *J. Appl. Meteor.,* **21,** 401–412.

Ebert, E., 1987: A pattern recognition technique for distinguishing surface and cloud types in the polar regions. *J. Climate Appl. Meteor.,* **26,** 1412–1427.

——, 1989: Analysis of polar clouds from satellite imagery using pattern recognition and a statistical cloud analysis scheme. *J. Appl. Meteor.,* **28,** 382–399.

Frey, R. A., B. A. Baum, W. P. Menzel, S. A. Ackerman, C. C. Moeller, and J. D. Spinhirne, 1999: A comparison of cloud top heights computed from airborne lidar and MAS radiance data using CO_2 slicing. *J. Geophys. Res.,* **104,** 24 547–24 555.

Garand, L., 1988: Automated recognition of oceanic cloud patterns. Part I: Methodology and application to cloud climatology. *J. Climate,* **1,** 20–39.

Haertel, V., and D. A. Landgrebe, 1999: On the classification of classes with nearly equal spectral response in remote sensing hyperspectral image data. *IEEE Trans. Geosci. Remote Sens.,* **37,** 2374–2385.

Inoue, T., 1985: On the temperature and effective emissivity determination of semi-transparent cirrus clouds by bispectral measurements in the 10 μm window region. *J. Meteor. Soc. Japan,* **63,** 88–99.

——, 1987: A cloud type classification with *NOAA-7* split-window measurements. *J. Geophys. Res.,* **92,** 3991–4000.

Key, J., 1990: Cloud cover analysis with arctic AVHRR data. Part II: Classification with spectral and textural measures. *J. Geophys. Res.,* **95,** 7661–7675.

——, J. A. Maslanik, and A. J. Schweiger, 1989: Classification of merged AVHRR and SMMR Arctic data with neural networks. *Photogramm. Eng. Remote Sens.,* **55,** 1331–1338.

Knottenberg, H., and E. Raschke, 1982: On the discrimination of water and ice clouds in multispectral AVHRR data. *Ann. Meteor.,* **18,** 145–147.

Lee, J. S., M. R. Grunes, T. L. Ainsworth, L. J. Du, D. L. Schuler, and S. R. Cloude, 1999: Unsupervised classification using polarimetric decomposition and the complex Wishart classifier. *IEEE Trans. Geosci. Remote Sens.,* **37,** 2249–2258.

Li, J., and F. Zhou, 1990: Computer indentification of multispectral satellite cloud imagery. *Adv. Atmos. Sci.,* **7,** 366–375.

——, ——, and L. Wang, 1992: Automatic classification and compression of GMS cloud imagery in heavy rainfall monitoring application. *Adv. Atmos. Sci.,* **9,** 458–464.

——, L. Wang, and F. Zhou, 1993: Convective and stratiform rainfall estimation from geostationary satellite data. *Adv. Atmos. Sci.,* **10,** 475–480.

——, W. P. Menzel, H. L. Huang, L. E. Gumley, S. A. Ackerman, and T. J. Schmit, 2001a: Atmospheric retrievals from MODIS measurements: A comparison with GOES sounder products. *Optical Remote Sensing of the Atmosphere: February 5–8, 2001, Coeur d'Alene, Idaho,* Optical Society of America, 97–99.

——, ——, and A. J. Schreiner, 2001b: Variational retrieval of cloud parameters from GOES sounder longwave cloudy radiance measurements. *J. Appl. Meteor.,* **40,** 312–330.

Lubin, D., and E. Morrow, 1998: Evaluation of an AVHRR cloud detection and classification method over the central Artic Ocean. *J. Appl. Meteor.,* **37,** 166–183.

Prabhakara, C., J. M. Yoo, D. P. Kratz, and G. Dalu, 1993: Boundary layer stratus clouds: Inferred from satellite infrared spectral measurements over oceans. *J. Quant. Spectrosc. Radiat. Transfer,* **49,** 559–607.

Rossow, W. B., and L. C. Garder, 1993: Validation of ISCCP cloud detections. *J. Climate,* **6,** 2370–2393.

——, and Coauthors, 1985: ISCCP cloud algorithm intercomparison. *J. Climate Appl. Meteor.,* **24,** 877–903.

Salisbury, J. W., and D. M. D'Aria, 1992: Emissivity of terrestrial materials in the 8–14 μm atmospheric window. *Remote Sens. Environ.,* **42,** 83–106.

Saunders, R. W., and K. T. Kriebel, 1998: An improved method for detecting clear sky and cloudy radiances from AVHRR data. *Int. J. Remote Sens.,* **9,** 123–150.

Seze, G., and M. Desbois, 1987: Cloud cover analysis from satellite imagery using spatial and temporal characteristics of data. *J. Climate Appl. Meteor.,* **26,** 287–303.

Strabala, K. I., S. A. Ackerman, and W. P. Menzel, 1994: Cloud properties inferred from 8–12-μm data. *J. Appl. Meteor.,* **33,** 212–229.

Susskind, J., C. D. Barnet, and J. Blaisdell, 1998: Determination of atmospheric and surface parameters from simulated AIRS/AMSU sounding data: Retrieval methodology and cloud clearing methodology. *Adv. Space Res.,* **21,** 369–384.

Tag, P. M., R. L. Bankert, and L. R. Brody, 2000: An AVHRR multiple cloud-type classification package. *J. Appl. Meteor.,* **39,** 125–134.

Tsonis, A. A., 1984: On the separability of various classes from GOES visible and infrared data. *J. Climate Appl. Meteor.,* **23,** 1393–1410.

Uddstrom, M. J., and W. R. Gray, 1996: Satellite cloud classification and rain-rate estimation using multispectral radiances and measures of spatial texture. *J. Appl. Meteor.,* **35,** 839–858.

Velden, C. S., C. M. Hayden, S. J. Nieman, W. P. Menzel, S. Wanzong, and J. S. Goerss, 1997: Upper-tropospheric winds derived from geostationary satellite water vapor observations. *Bull. Amer. Meteor. Soc.,* **78,** 173–195.

Vemury, S., L. L. Stowe, and V. R. Anne, 2001: AVHRR pixel level clear-sky classification using dynamic thresholds (CLAVR-3). *J. Atmos. Oceanic Technol.,* **18,** 169–186.

Welch, R. M., S. K. Sengupta, A. K. Goroch, P. Rabindra, N. Rangaraj, and M. S. Navar, 1992: Polar cloud and surface classification using AVHRR imagery: An intercomparison of methods. *J. Appl. Meteor.,* **31,** 405–420.